

*Ion-electron recombination
in merged-beams experiments*

Henning T. Schmidt

Institute of Physics and Astronomy,
Aarhus University.

1994

Table of Contents

1.	Preface	2
2.	Introduction	6
3.	The Merged-Beams Experiments	9
	3.1. <i>The ion beams</i>	10
	3.2. <i>The electron beams</i>	14
	3.3. <i>Electron cooling</i>	29
4.	Radiative Recombination	35
	4.1 <i>RR for fully stripped ions</i>	35
	4.2 <i>RR for non-fully stripped ions</i>	39
	4.3 <i>Laser induced RR</i>	42
5.	Dielectronic Recombination	47
	5.1 <i>Introduction to DR</i>	47
	5.2 <i>DR for ground state Li-like ions</i>	52
	5.3 <i>DR for metastable He-like ions</i> <i>(the single-pass experiment)</i>	57
	5.4 <i>DR for metastable He-like ions</i> <i>(the TSR experiment)</i>	67
	5.5 <i>DR for Be-, B-, and C-like ions</i>	74
6.	Lifetime measurements based on DR	77
	6.1 <i>Lifetime of the 3S metastable state of He-like ions</i>	77
	6.2 <i>The experiment</i>	79
	6.3 <i>Analysis of data from the decay rate measurement</i>	82
	6.4 <i>Discussion of the results</i>	88
7.	Dissociative Recombination	94
	7.1 <i>Earlier DisR experiments</i>	94
	7.2 <i>Some basic concepts of diatomic molecules</i>	96
	7.3 <i>The DisR processes</i>	101
	7.4 <i>The ASTRID H_2^+ experiment</i>	106
	7.5 <i>Results and discussion</i>	112
8.	Summary	121
9.	Dansk resumé	123
10.	Acknowledgments	125

1. Preface

The present thesis serves to fulfil the requirements for the Ph.D. degree at the Faculty of Natural Sciences, Aarhus University. The thesis presents merged-beams experiments, investigating processes of ion-electron recombination. The main part of the work described was performed with the electron cooler at the Institute of Physics and Astronomy, Aarhus University, but the results of a six-month stay at the Max-Planck-Institut (MPI) für Kernphysik in Heidelberg, Germany, are presented as well.

When in the mid-80s, it was decided to build the Aarhus Storage Ring, Denmark (ASTRID), a wise and fruitful decision of building first the electron cooler and installing it at the TANDEM accelerator was made. This way one could gain experience working with ultra-high vacuum systems before constructing the storage ring itself, and at the same time provide an excellent tool for the study of recombination between free electrons and multiply charged ions in a single-pass configuration. Indeed, impressive results were obtained. The first direct tests of the absolute cross sections for radiative recombination (RR) were performed (Andersen 1990), and the dielectronic recombination (DR) measurements (Andersen 1989) had an energy resolution improved by a factor of 30 compared to earlier works.

When I joined the project as a student in the Fall of 1989, these two great successes had been achieved quite recently, and in the spirit of optimism that followed, we decided to try to perform laser-induced radiative recombination (LIR). This attempt was not successful, and after observations of LIR were reported from MPI, Heidelberg

(Schramm 1991) and from University of Western Ontario (Yousif 1991), we stopped this experiment. During the time of our LIR experiment, we continued to study RR for non-fully stripped ions [II,V] and DR with low-energy electrons [I,III,IV,V]. In the Spring of 1992, the electron cooler was 'recombined' with ASTRID. In the following year, technical difficulties had to be solved, and no real electron-cooler experiments were performed. During this year, I spent six months in Heidelberg working on DR with metastable He-like ions measured both as a function of electron energy and as a function of time after injection to deduce the lifetimes of the metastable $1s2s\ ^3S$ states [VI]. In 1993 we made the first experiments with the electron cooler at ASTRID. So far, we have studied electron cooling of D^+ , dissociative recombination (DisR) of H_2^+ , and electron-impact detachment of D^- . For future applications of the electron cooler, we have improved the energy resolution at low relative energies by about one order of magnitude, applying the so-called 'adiabatic expansion' technique first realized at the Stockholm storage ring CRYRING (Danared 1993).

Throughout this thesis, a rather significant variation concerning the amount of details presented on the performance and results of the different experiments will encounter the reader. This is due to a selection based on the following criteria: First of all, previously unpublished material, in particular sec.5.4 on the TSR measurement of DR for metastable He-like ions and ch.7 on the ASTRID experiment on DisR of H_2^+ , is given a high priority. Other criteria also considered in the selection process are the existence of detailed theoretical predictions to compare with our data and the usefulness of a certain

detail in making a point in the presentation.

Parts of the material considered in this thesis has previously been presented in the publications listed in the following.

- I. N R Badnell, M S Pindzola, L H Andersen, J Bolko, and H T Schmidt (1991): *Dielectronic recombination of light Be-like and B-like ions*. Journal of Physics B **24** 4441
- II. L H Andersen, G Y Pan, and H T Schmidt (1992): *Radiative recombination with highly charged Si^{6+} and Si^{11+} ions*. Journal of Physics B **25** 277
- III. L H Andersen, G Y Pan, H T Schmidt, N R Badnell, and M S Pindzola (1992): *State-selective measurements and calculations of dielectronic recombination with Li-like N^{4+} , F^{6+} and Si^{11+} ions*. Physical Review A **45** 6332
- IV. L H Andersen, G Y Pan, H T Schmidt, N R Badnell, and M S Pindzola (1992): *Absolute measurements and calculations of dielectronic recombination with metastable He-like N, F and Si ions*. Physical Review A **45** 7868
- V. H T Schmidt, G Y Pan, and L H Andersen (1992): *Dielectronic recombination with $\Delta n=0$ and $\Delta n=1$ core excitations and radiative recombination for C-like F^{3+} ions*. Journal of Physics B **25** 3165
- VI. H T Schmidt, P Forck, M Grieser, D Habs, J Kenntner, G Miersch, R Repnow, U Schramm, T Schüßler, D Schwalm, and A Wolf (1994): *High-precision measurement of the relativistic magnetic-dipole decay rate of metastable heliumlike carbon ions in a storage ring*. Phys.Rev.Lett. **72**, 1616

The papers listed above will be referred to by roman numbers, whereas other literature cited in the text is referred to by the name of the first author followed by the year of publication. References to other literature will be given at the end of each chapter.

L H Andersen, J Bolko, P Kvistgaard (1990) Phys.Rev.Lett. 64 729.

L H Andersen, P Hvelplund, H Knudsen, and P Kvistgaard (1989) Phys.Rev.Lett. 62 2656

U Schramm, J Berger, M Grieser, D Habs, E Jaeschke, G Kilgus, D Schwalm, A Wolf, R Neumann, R Schuch (1991) Phys.Rev.Lett. 67 22

F B Yousif, P v.d. Donk, Z Kucherowski, J Reis, E Brannen, J B A Mitchell, and T J Morgan (1991) Phys.Rev.Lett. 67 26

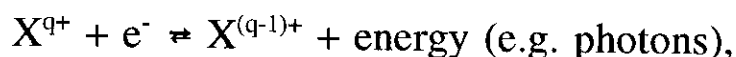
H Danared (1993) NIM A335 397

2. Introduction

From our every-day experience, we all know that matter is found in three phases: The solid phase, the liquid phase, and the gaseous phase. In the ordinary gas phase, matter consists of free neutral molecules. In the situation, where some degree of ionization has taken place, and we have a mixture of atomic and molecular ions and free electrons, we speak of a fourth phase, the plasma phase.

The plasma phase can be reached either by having a very high temperature or by introducing some external ionization mechanism, such as an electrical discharge or irradiation with light with a photon energy exceeding a few eV (i.e. UV, x rays, and γ rays).

When a plasma has been formed, an equilibrium situation can be reached:



where X^{q+} denotes an ion in charge state $q+$. The process from right to left is ionization, while the inverse process is ion-electron recombination, the subject of this thesis. Of course, in a plasma many other processes take place (ion-ion charge exchange, ion excitation induced by collisions with electrons, emission of bremsstrahlung from electrons accelerated by ions, etc.). However, ion-electron recombination remains an essential feature of plasma physics. Plasmas, where these 'atomic physics' processes are dominating, are well known in nature. They can be found in, e.g., stellar atmospheres and in interstellar nebulae; but also in the upper atmosphere of the Earth, where the solar UV radiation leads to ionization. In fact, some of the first experimental

investigations of ion-electron recombination were performed as an attempt to understand the number densities of atomic and molecular ions in the upper atmosphere.

Let us now consider a system consisting of an ion X^{q+} and a free electron e^- . By the conventional definition of the zero point for the total mechanical energy, this system must have a positive energy, while a system forming a stable, bound state of the two (i.e. $X^{(q-1)+}$) must have a negative energy. Hence, in a recombination process, energy in some form must be released. In radiative recombination (RR), the excess energy is emitted in the form of a photon. This is a non-resonant process, having its maximum rate at 0 eV relative energy. Since this process does not require any change of the structure of the initial ion, this will be possible for any positive ion, even a fully stripped one. Another process, also possible for any ion, is referred to as three-body (or ternary) recombination (TR). In this process, the excess energy is given to a second free electron in the form of kinetic energy. Since this process requires the presence of two free electrons, it will have a rate proportional to the electron density n_e squared. This means that when the electron density becomes sufficiently high, the TR rate (which also takes on its maximum value at zero relative energy) will exceed the RR rate. However, for the experiments described in this thesis, the electron density is sufficiently low that the TR contribution is negligible.

For ions carrying electrons, a third recombination mechanism, known as dielectronic recombination (DR), becomes possible. Here the excess energy in the recombination process is used to excite one of the bound electrons, leaving the ion in a doubly excited state which might

autoionize or, alternatively, stabilize radiatively, in which case the DR process has been completed. Since the excitation of the initially bound electron requires a specific amount of energy, the DR process will be resonant.

When the ion, in the initial state, is a molecular ion, new degrees of freedom describing the relative motion of the nuclei are introduced. This makes possible a fourth recombination mechanism, for which the excess energy is transferred to these new degrees of freedom. As a consequence of this, the molecule dissociates. This process is therefore called dissociative recombination.

3. The Merged-Beams Experiments

In this chapter, general features of the merged-beams experiments will be described, postponing some experimental points to the chapters concerning the particular experiments. In sec.3.1 the accelerators and ion beams are briefly described, emphasizing the features relevant to the electron-cooler experiments. Section 3.2 deals with the electron cooler. The electron beam will be described in much more detail than the ion beam since it is the velocity spread of the electrons that determines the energy resolution in the experiments. The final section of this chapter is devoted to electron cooling which, besides being an interesting physical process in itself, is an important tool for understanding other merged-beams experiments performed in storage rings.

The general idea of merged-beams recombination measurements is to overlap two co-propagating beams of electrons and ions of charge q times the elementary charge e over a certain interaction region, and then, as a function of the relative energy, monitor the yield of ions in charge state $(q-1)+$. The entity determined in the experiments is the recombination rate coefficient $\langle v\sigma \rangle$ (see sec.3.2 eq.3.5). The experimental rate coefficient is determined as

$$\langle v\sigma \rangle = \frac{N^{(q-1)+} - N_0^{(q-1)+}}{N^{q+}} \frac{v_i}{\text{Ln } \epsilon}, \quad (3.1)$$

where $N^{(q-1)+}$ is the yield of ions in the $(q-1)+$ charge state, with the electron beam tuned to the desired relative energy, $N_0^{(q-1)+}$ is a background measurement performed by switching off the ion beam (chopping), or changing the energy to a value with zero rate coefficient

(modulating) or, in the case of the storage ring, DR measurements for ions in metastable states waiting for the metastable component to decay to the ground state. L is the length of the interaction region, n_e is the electron density, ϵ is the detector efficiency, and v_i is the ion velocity in the laboratory rest frame.

3.1. The ion beams

The single-pass experiments [I-V] were performed at the Aarhus 6 MV Tandem accelerator. The setup is sketched in fig. 3.1. Positively charged atomic ions were available with typical currents in the range of 200 nA to about 1 μ A for energies of 1-2 MeV per atomic mass unit. From the bending magnet before the electron cooler and on, the pressure was kept below $1\text{-}2 \cdot 10^{-11}$ mBar to reduce the background signal caused by electron capture in collisions with residual-gas molecules. In the interaction region, two sets of electro-static pick-up

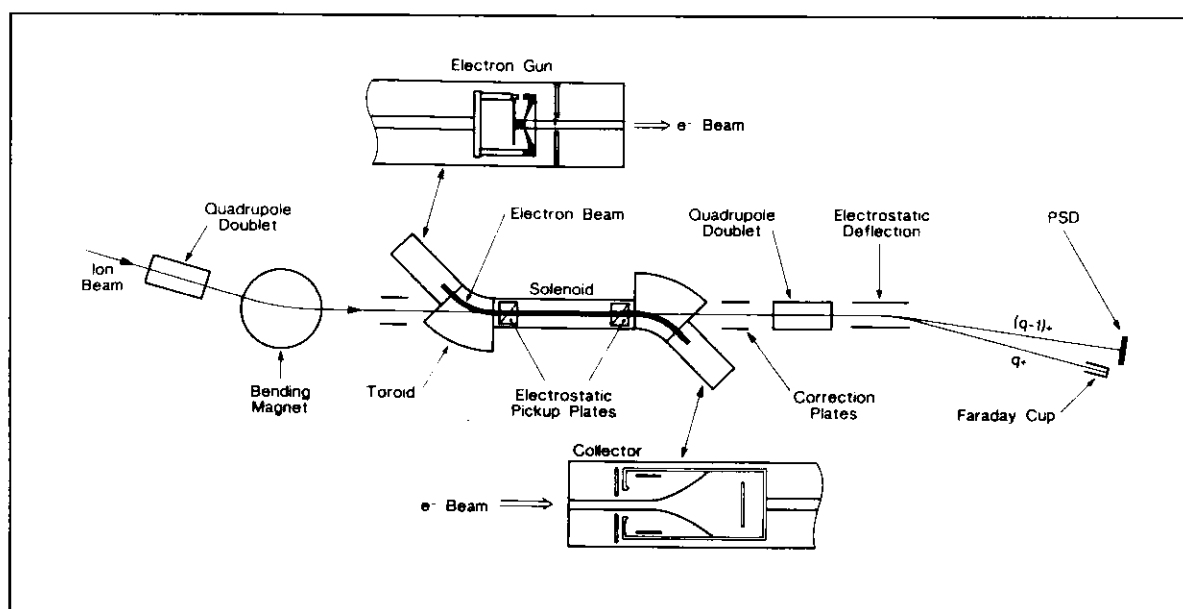


Figure 3.1 *The Aarhus single-pass experiment.*

plates were used to monitor the positions of both the ion and electron beams to ensure full overlap. The ion beam was assumed to be gaussian with a FWHM of 2-3 mm, and the electron beam was 1 cm diameter with uniform density. After the electron cooler, a charge-state separation was performed using a transverse electric field, typically of the order of 10 kV/cm. As a consequence of the traversal of this field, electrons in high Rydberg states were field-ionized and therefore not counted as recombined. The critical principal quantum number, n_{limit} , above which ionization takes place, is given by the following semi-classical expression (Griffin 1989)

$$n_{\text{limit}} = (6.2 \cdot 10^8 q^3/E)^{1/4}, \quad (3.2)$$

where E is the electric-field strength in V/cm. To facilitate the detection, it was necessary to focus the final-state ions onto the position-sensitive channel-plate detector, and therefore no experiments with singly charged ions could be performed since these would result in neutral products.

Figure 3.2 shows the storage ring ASTRID with the parts of greatest interest to the electron-cooler experiments. Beams of singly charged, positive and negative, atomic and molecular ions covering a mass range of 1-1000 atomic mass units have been stored at the injection energy of 50 to 200 keV. However, to perform electron cooler experiments, it is necessary to increase the energy to several MeV, depending on the specific ion beam. The acceleration is achieved by bunching the beam with the RF cavity and then perform a synchronized ramping of the magnetic-dipole fields of the storage ring and the RF frequency. During this ramping, it is necessary to monitor the

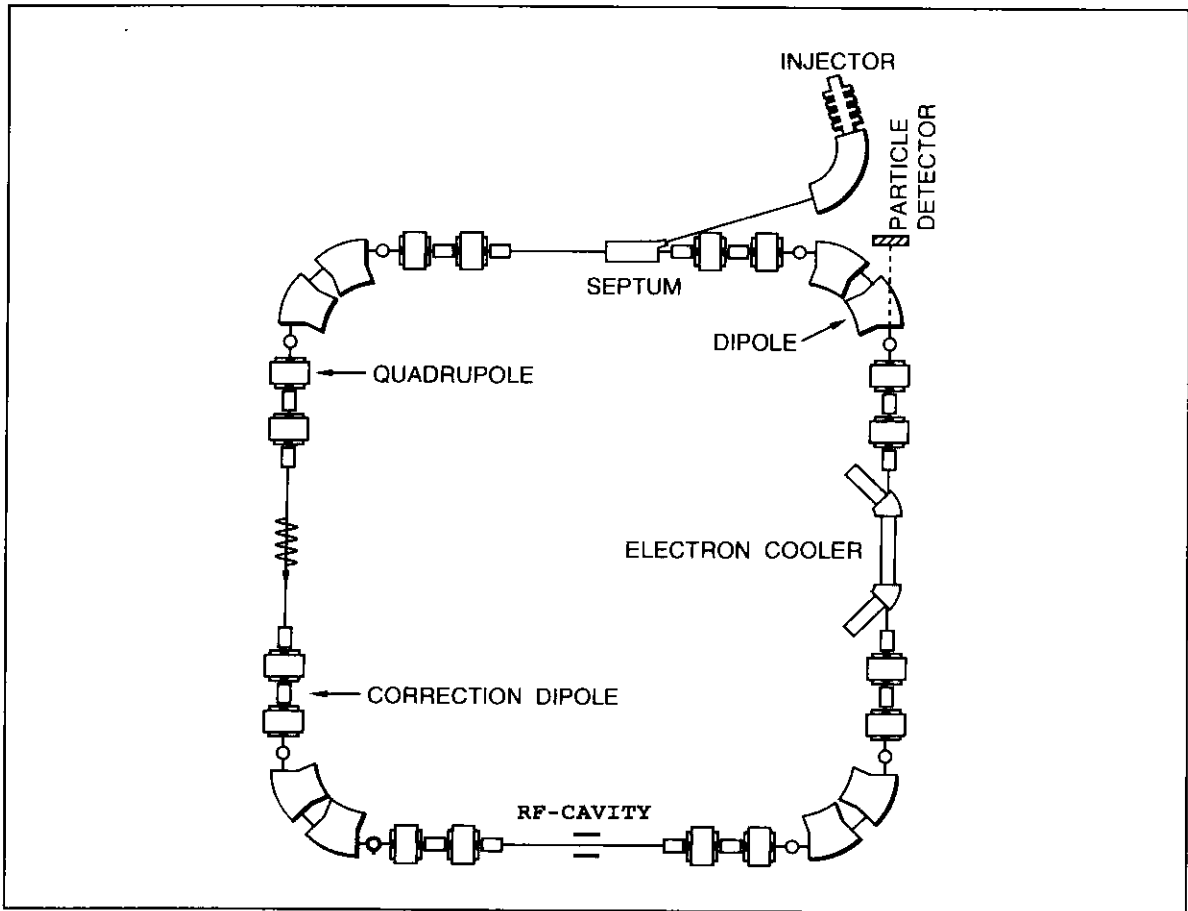


Figure 3.2 *The ASTRID storage ring.*

time structure of the ion beam on one of the pick-up plates to keep the relative phase of the RF and the ion bunches fixed. To perform this monitoring, an ion current of 0.5-1 μA is required. Due to losses during storage and acceleration, it is therefore only possible to perform electron-cooler experiments with ions for which currents from the ion sources of a few μA 's are achievable. For many singly charged positive ions, currents of this magnitude are available from the 'universal' standard plasma ion sources ('Nielsen'-sources). For some negative ions, sputter ion sources (e.g. O^-) or duoplasmatrons (e.g. H^-) can yield the necessary current. An EBIS (Electron Beam Ion Source) that can yield high currents of multiply charged ions is under construction and will be available for future experiments. The ion-beam

position is monitored by the ten sets of electrostatic pick-up plates; two in the electron cooler and one at each end of the four straight sections. The positions can be optimized by adjusting the eight correction dipoles. Charge-state analysis is inherently performed in the dipole magnet following the electron cooler. The effective electric field caused by the transverse magnetic field will lead to field ionization of ions in high Rydberg states according to eq.(3.2). In SI units, the field strength is given as

$$E = \gamma v B = \frac{v B}{\sqrt{1 - v^2/c^2}}, \quad (3.3)$$

where v is the ion velocity. This electric field is typically of the order of 100 kV/cm.

As mentioned in the preface, some of the experiments described in this thesis were performed at the TSR (Test Storage Ring) at the Max-Planck-Institut für Kernphysik in Heidelberg. At the TSR, ions can be injected from a 12 MV Tandem accelerator. This means that electron-cooler experiments can be performed at the injection energy. This point was crucial to these experiments since they concerned ions in metastable states with lifetimes in the millisecond range, leaving no time for ion-beam acceleration. Like in ASTRID, the dipole magnet following the electron cooler acts as a charge-state analyzer. This means that field ionization according to eqs. (3.2) and (3.3) takes place.

3.2 The electron beams

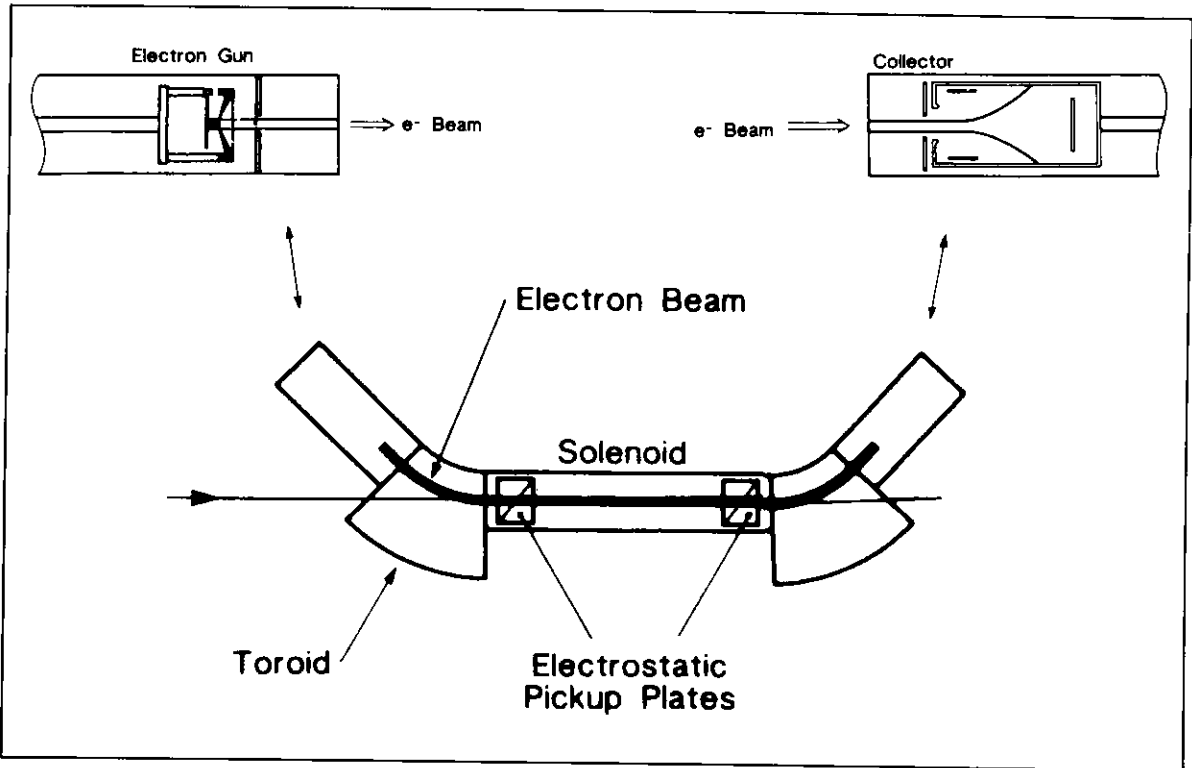


Figure 3.3 *The ASTRID electron cooler.*

Figure 3.3 shows schematically the ASTRID electron cooler. The source of electrons is an indirectly heated disc-shaped BaO-coated tungsten cathode. Cathodes of 10 and 15 mm diameter have been used. The cathode is surrounded by a Pierce shield which can be given a low bias voltage with respect to the cathode potential. From the cathode, the electrons are accelerated towards the anode which is a grid with approximately 80% transmittance. In the case of a space-charge-limited electron beam, the emitted electron current is given by (Poth 1990)

$$I_{\text{electron}} = PV^{3/2}, \quad (3.4)$$

where V is the cathode-anode potential difference, and the constant of proportionality P (the perveance) is inversely proportional to the square

of the cathode-anode distance which can be varied from the outside, allowing for continuous electron-current tuning. The electron beam is guided from the electron gun through the one-meter interaction region to the collector by a solenoid magnetic field. In standard operation, this field is kept constant from the electron gun to the entrance of the collector, leading to a constant beam diameter equal to the cathode diameter. In the collector, the solenoid field decreases, and the beam blows up transversely.

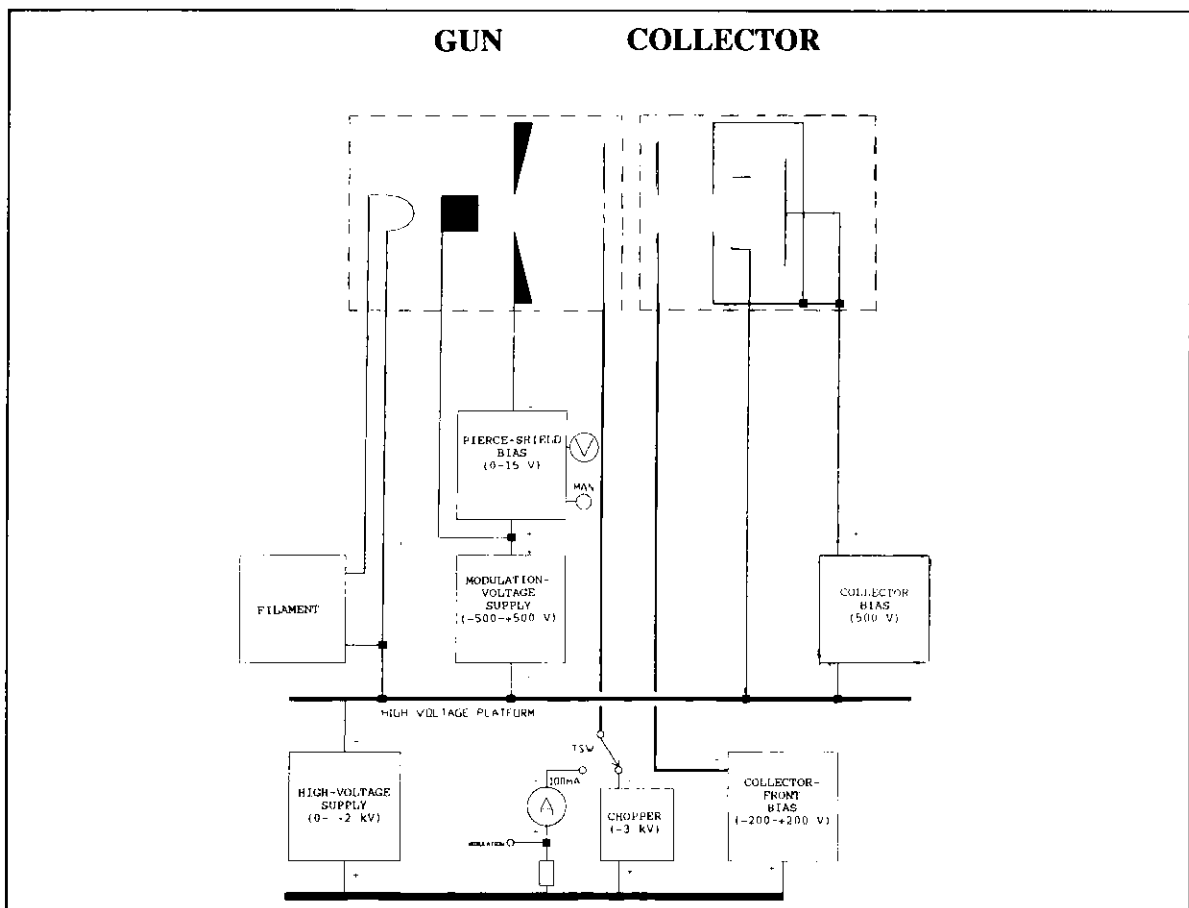


Figure 3.4 *The electrical connections for the electron cooler.*

In fig.3.4 is shown the electrical connections for the electron cooler. The cooler can be run in a DC mode, where the high-voltage platform voltage is equal to the acceleration voltage, but it is often useful to be able to modulate the acceleration voltage between two

values or to switch the beam on and off. For modulation, we have a ± 500 V supply at the high-voltage platform, and for chopping the beam we have a 3 kV supply connected to the anode.

In the remainder of this section, I will discuss the electron-beam velocity distribution since the influence of the ion-velocity distribution on the distribution of relative velocities can be neglected due to the much larger mass of the ions. If the total cross section for recombination as a function of the relative velocity v is known, the rate coefficient $\langle v\sigma \rangle$ in a merged-beams experiment may be expressed as

$$\langle v\sigma \rangle = \int v \sigma(v) f(\bar{v}, \Delta, T_{\perp}, T_{\parallel}) d\bar{v}. \quad (3.5)$$

Here the electron-velocity distribution f in the ion-beam rest frame is a flattened Maxwell distribution, i.e., the product of a two-dimensional transverse and a one-dimensional longitudinal, gaussian velocity distribution,

$$f(\bar{v}, \Delta, T_{\perp}, T_{\parallel}) = \frac{m}{2\pi k T_{\perp}} \exp\left(\frac{-mv_{\perp}^2}{2kT_{\perp}}\right) \cdot \left(\frac{m}{2\pi k T_{\parallel}}\right)^{1/2} \exp\left(\frac{-mv_{\parallel}^2}{2kT_{\parallel}}\right), \quad (3.6)$$

where v_{\parallel} and v_{\perp} are the *random* components of the relative velocity parallel and perpendicular to the ion-beam direction, respectively, T_{\parallel} and T_{\perp} are the associated 'temperatures' of the electron beam, and Δ is the detuning velocity. The relative velocity is related to the detuning velocity through the following 'pythagorean' relation:

$$v^2 = v_{\perp}^2 + (\Delta + v_{\parallel})^2. \quad (3.7)$$

The deviation of the relative energy E_{rel} from the value $E_{\text{rel},0} = m\Delta^2/2$ is

then found to be

$$\delta E_{\text{rel}} = m(v^2 - \Delta^2)/2 = \delta E_{\perp} + \delta E_{\parallel} \pm 2\sqrt{E_{\text{rel},0}} \delta E_{\parallel}, \quad (3.8)$$

where $\delta E_{\perp} = mv_{\perp}^2/2$. For typical electron-beam temperatures of $kT_{\perp} = 100$ meV and $kT_{\parallel} = 1$ meV, we see from eq.(3.8) that for low energies ($E_{\text{rel}} \leq 1$ eV), kT_{\perp} determines the energy resolution, whereas for $E_{\text{rel}} \geq 10$ eV, the last term in eq.(3.8) dominates, and kT_{\parallel} determines the resolution. When low relative energies are considered (i.e. electron-cooling experiments, radiative recombination, dissociative recombination, and low-energy dielectronic recombination), it is therefore of interest to reduce kT_{\perp} .

When the guiding solenoid field is kept constant through the cooler, $kT_{\perp} \approx kT_{\text{cath}}$, where T_{cath} is the temperature of the cathode. One way to reduce kT_{\perp} is then to reduce the temperature of the cathode. At the MPI Heidelberg, experiments have been made with electron beams produced by laser irradiation of a cold semi-conductor cathode (Habs 1988), but so far, sufficient current for electron-cooler operation has not been achieved. Another way of reducing kT_{\perp} is the so-called adiabatic expansion technique, where the magnetic field strength of the guiding solenoid decreases slowly from the electron gun to the interaction region, leading to an almost proportional decrease in kT_{\perp} (Danared 1993). Since we are now applying the second of these methods, I will describe this in more detail.

Because of the guiding magnetic field, the energy in the transverse motion caused by the finite temperature of the cathode, and possibly imperfections in the fields will be 'stored' in the cyclotron motion of the electrons. The energy in the cyclotron motion is given by the subscript c (for cyclotron)

$$E_c = m r_c^2 \omega_c^2 / 2 = B^2 r_c^2 e^2 / (2m). \quad (3.9)$$

If we assume that the relative change in r_c during one cyclotron oscillation is much smaller than unity (adiabatic motion), the electrons will be able to follow the magnetic field lines, and the magnetic flux through a cyclotron loop will be constant. Hence $B r_c^2$ is constant. Comparing this to eq.(3.9), we find that E_c changes proportional to the magnetic field. As a measure of the adiabaticity, we introduce the adiabaticity parameter χ , defined by

$$\chi = \frac{1}{B} T \frac{dB}{dt} = \frac{1}{B} \lambda_c \frac{dB}{dz}, \quad (3.10)$$

where T is the cyclotron period, z is the position coordinate along the beam axis, and the distance travelled in the z direction during one period, λ_c , is given by

$$\lambda_c = \left(\frac{8\pi^2 m E_0}{e^2 B^2} \right)^{1/2}, \quad (3.11)$$

where E_0 is the electron-beam energy. Numerical simulations using the Hermansfeldt computer code (Hermansfeldt 1979) show that the motion remains adiabatic up to $|\chi_{\max}| \approx 0.35$. The new ASTRID gun solenoid can give a magnetic field of 2 kG. The magnetic field on axis and the adiabaticity parameter are shown in fig.3.5 for an electron energy of 1 keV and interaction magnetic fields of 100 G and 200 G.

So far, I have assumed that the transverse motion of the electrons consisted solely of the circular motion caused by the random velocity component perpendicular to the solenoid field. This is not strictly true: Even if an electron is launched from the gun with zero

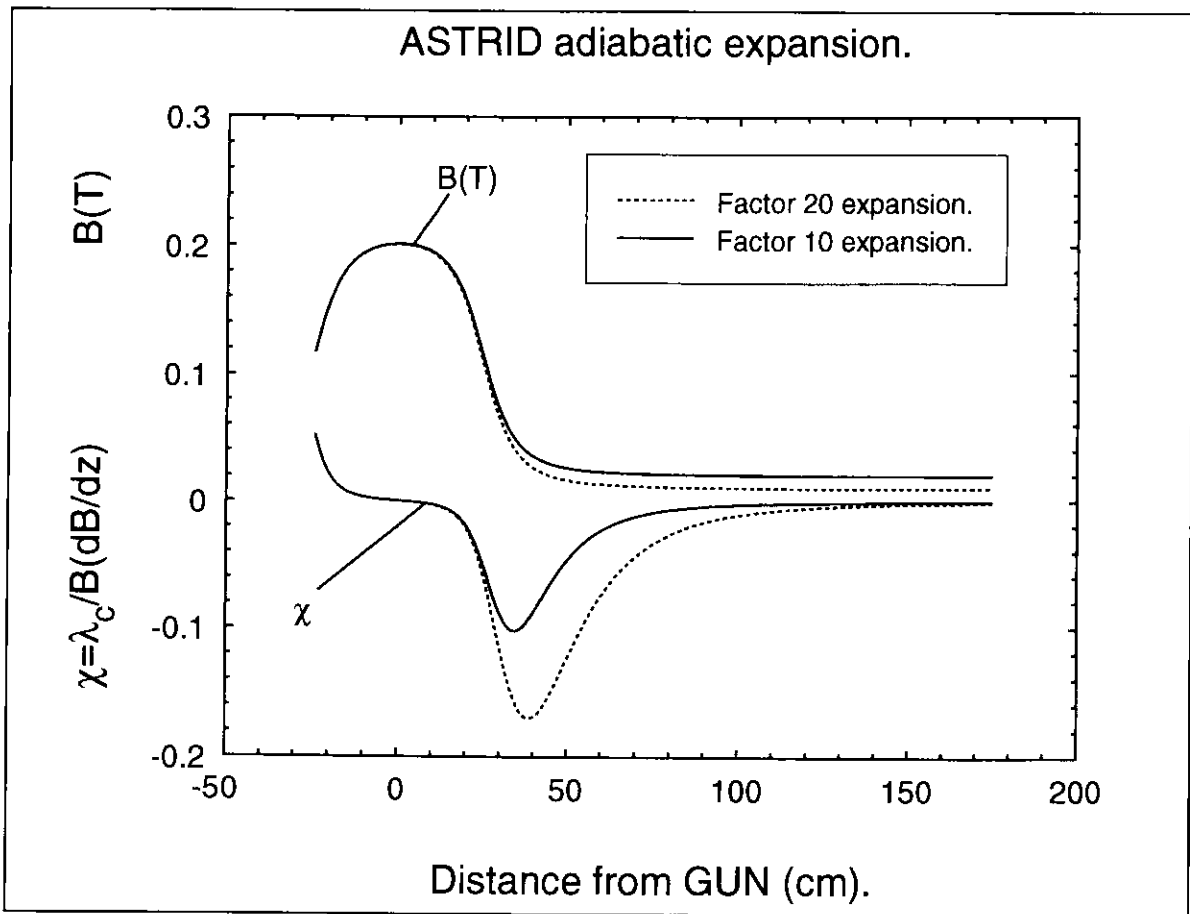


Figure 3.5

transverse velocity, it will start to perform the transverse so-called steady motion. The steady motion is caused by the space-charge electric field, in combination with the solenoid field, and its energy is given by (Poth 1990)

$$E_{ST} = \frac{mr^2\omega_p^4}{8\omega_c^2\gamma^2}, \quad (3.12)$$

where r is the distance from the center of the beam, ω_p is the plasma frequency, and γ is the relativistic Lorentz factor which is close to one for the energy range of about 1 keV of interest to us. A convenient formula for the steady motion energy yields

$$E_{ST}(\text{eV}) = 2.3 \cdot 10^{-14} \left(\frac{r(\text{mm})n_e(\text{cm}^{-3})}{B(\text{G})} \right)^2, \quad (3.13)$$

where n_e is the electron density. Normally $E_{ST} \ll E_c$, but since E_{ST} in the interaction region depends only on the value of the parameters r , B , and n_e in the interaction region, E_{ST} is not affected by the adiabatic expansion and hence sets a limit to the usefulness of this technique. In table 3.1 are shown the cyclotron and steady-motion energies for an electron launched from the gun with a typical transverse energy of 0.13 eV, assuming an interaction-region electron density of $n_e = 5 \cdot 10^6 \text{ cm}^{-3}$.

Table 3.1

Expansion factor	$E_c(\text{meV})$	$E_{ST}(\text{meV})$ $r=5\text{mm}$	$E_{ST}(\text{meV})$ $r=10\text{mm}$	$E_{ST}(\text{meV})$ $r=15\text{mm}$	$E_{ST}(\text{meV})$ $r=20\text{mm}$
10	13	0.4	1.7	3.6	*)-
20	6.5	1.7	6.8	15	23

*) *The 1 cm diameter cathode is used. Therefore the radius after a factor of 10 expansion is only 15.8 mm.*

As can be seen from eq.(3.8), also the longitudinal electron-beam temperature plays a role in determining the energy resolution for $E_{rel} \geq 1 \text{ eV}$, in particular if the transverse-energy spread is decreased by adiabatic expansion. We therefore now turn to the longitudinal electron-beam temperature kT_l . Electrons emitted from the hot BaO-coated tungsten cathode obey a spherically symmetric maxwellian velocity distribution with temperature T_{cath} . The ripple on the acceleration voltage causes an increase in the longitudinal-energy spread, as

observed in the laboratory rest frame. What is interesting from the point of view of the experiments is, however, the velocity distribution in the reference frame moving with the average electron velocity. After transforming to this frame of reference, one finds the following longitudinal temperature (Poth 1990):

$$kT_{\parallel} = \frac{(eV_{\text{ripple}} + kT_{\text{cath}})^2}{4E_0}, \quad (3.14)$$

where E_0 denotes the electron-beam energy.

The longitudinal temperature given above is, however, not the temperature one finds in the interaction region. In particular, the heating mechanisms, known as longitudinal-longitudinal relaxation and transverse-longitudinal relaxation, play a decisive role in determining the longitudinal beam temperature in the interaction region. These two mechanisms will be described in the following.

When the electrons leave the cathode, their spatial distribution will not be uniform. This means that they will have different potential energies determined by the local density of electrons. The phase-space compression caused by the acceleration as indicated in the above formula will, if the electrons are given sufficient time prior to the acceleration to have these variations in potential energy evolve into kinetic-energy variations, make the effect of this mechanism become negligible. If, however, the acceleration is fast compared to the typical plasma time scale, $\tau_p = 2\pi/\omega_p$, where the plasma frequency is given by $\omega_p = \sqrt{4\pi n_e e^2/m}$, the spatial fluctuations will survive until after the acceleration, whereupon this so-called longitudinal-longitudinal relaxation will lead to an increase of the longitudinal temperature of

approximately $e^2 n_e^{1/3}$ (Kudelainen 1982).

The electron beam now produced has a highly oblate velocity distribution ($kT_{\parallel} \ll kT_{\perp}$). In this beam elastic scattering among the electrons will gradually transfer the velocity spread from the transverse degrees of freedom into the longitudinal degree of freedom until eventually $kT_{\parallel} = kT_{\perp}$. If the influence of the guiding magnetic field is neglected, the rate of transverse-longitudinal relaxation pr. unit length is given by (Dikansky 1987)

$$\left(\frac{d(kT_{\parallel})}{dz} \right)_{B=0}^{t-1} = \frac{\pi e^3 j L_c C}{E_0} \sqrt{\frac{m}{kT_{\perp}}}, \quad (3.15)$$

where j is the current density, C is a numerical constant equal to 0.87 for an oblate maxwellian distribution, and L_c is the Coulomb logarithm:

$$L_c = \log \left(\frac{v_{\perp} / \omega_p}{e^2 / kT_{\perp}} \right). \quad (3.16)$$

In more convenient units, the rate of change in the longitudinal temperature is given by

$$\left(\frac{d(kT_{\parallel})}{dz} \right)_{B=0}^{t-1} = \frac{j(\text{A/cm}^2) L_c}{E_0(\text{eV}) \sqrt{kT_{\perp}(\text{eV})}} 8.46 \cdot 10^{-3} \text{eV/cm}. \quad (3.17)$$

The magnetic field restricts the transverse motion of the electrons to distances of the order of the cyclotron radius,

$$r_c = \frac{\sqrt{2mkT_{\perp}}}{eB} = 3.37 \text{ cm} \frac{\sqrt{kT_{\perp}(\text{eV})}}{B(\text{G})}. \quad (3.18)$$

For strong magnetic fields, $r_c \ll n_e^{-1/3}$ and collisions among electrons become improbable, leading to a suppression of the transverse-longitudinal relaxation mechanism. A quantitative measure of this suppression is given by an empirical formula (Kudelainen 1982, Dikansky 1987)

$$\left(\frac{d(kT_{\parallel})}{dz} \right)^{t-1} = \left(\frac{d(kT_{\parallel})}{dz} \right)_{B=0}^{t-1} \exp \left(-2.8 \frac{e^2/r_c}{e^2 n_e^{1/3} + kT_{\parallel}} \right). \quad (3.19)$$

I now want to evaluate the effect of these two heating mechanisms for various configurations relevant to the ASTRID electron cooler. We first consider the time scales involved.

We consider as an example an electron beam accelerated to $E_0=1000$ eV over a distance of $d=2$ cm and transported $s=1$ m.

$$\text{Acceleration time: } \tau_{\text{acc}} = 2d/v = 2.2 \text{ ns.}$$

$$\text{Plasma time scale: } \tau_p = 2\pi/\omega_p = 35 \text{ ns}/\sqrt{n_e/1 \cdot 10^7 \text{ cm}^{-3}}.$$

$$\text{Transport time: } \tau_{\text{tr}} = s/v = 52 \text{ ns.}$$

Since $\tau_{\text{acc.}} \ll \tau_p$, the acceleration is not adiabatic, and we have to take the longitudinal-longitudinal relaxation into account. As the transport time is of the order of the plasma time scale, we will add the extra longitudinal temperature gradually. A reasonable way to do this is to

set the rate of change of kT_{\parallel} due to longitudinal-longitudinal relaxation equal to

$$\left(\frac{d(kT_{\parallel})}{dz} \right)^{1-1} = \frac{e^2 n_e^{1/3}}{v\tau_p} \quad (3.20)$$

for $z < v\tau_p$ and otherwise zero.

Table 3.2

	Tandem	ASTRID (no ad.exp.)	ASTRID (ad.exp.x 20)	ASTRID (ad.exp.x 10)
Energy(eV)	1000	1000	1000	1000
Ripple peak-peak (V)	0.8	0.8	0.8	0.8
kT_{cath} (eV)	0.11	0.11	0.11	0.11
I (mA)	10	2.8	24.5	12.3
j^{GUN} (mA/cm ²)	12.7	1.56	31	15.6
n_e^{GUN} (cm ⁻³)	$4.1 \cdot 10^7$	$5 \cdot 10^6$	$1 \cdot 10^8$	$5 \cdot 10^7$
B^{GUN} (G)	100/200	100/200	2000	2000
$B^{\text{INT.}}$ (G)	–	–	100	200
$j^{\text{INT.}}$ (mA/cm ²)	–	–	1.56	1.56
$n_e^{\text{INT.}}$ (cm ⁻³)	–	–	$5 \cdot 10^6$	$5 \cdot 10^6$
$kT_{\parallel}^{\text{GUN}}$ (eV)	$6.5 \cdot 10^{-5}$	$6.5 \cdot 10^{-5}$	$6.5 \cdot 10^{-5}$	$6.5 \cdot 10^{-5}$
$kT_{\parallel}^{\text{INT.}}$ (eV) *)	$4.5/4.1 \cdot 10^{-4}$	$1.3/1.2 \cdot 10^{-4}$	$2.5 \cdot 10^{-4}$	$1.6 \cdot 10^{-4}$
kT_{\perp} (eV)	0.11	0.11	0.0055	0.011

*) *Halfway through the electron cooler.*

If we now add the contributions from longitudinal-longitudinal and transverse-longitudinal relaxation, we find the total rate of change of the longitudinal temperature. A numerical integration can then be performed to find the longitudinal temperature as a function of the distance from the electron-gun anode. The results of this calculation for some relevant configurations are given in table 3.2. Note that due to the lower electron density in the ASTRID experiments as compared to the Tandem experiments, the longitudinal temperature is expected to be lower.

Figure 3.6 shows the calculated electron beam temperatures for the ASTRID electron cooler in the case of a factor 10 adiabatic expansion as a function of the longitudinal-position coordinate z .

The electron-beam temperatures, kT_{\parallel} and kT_{\perp} , can be deter-

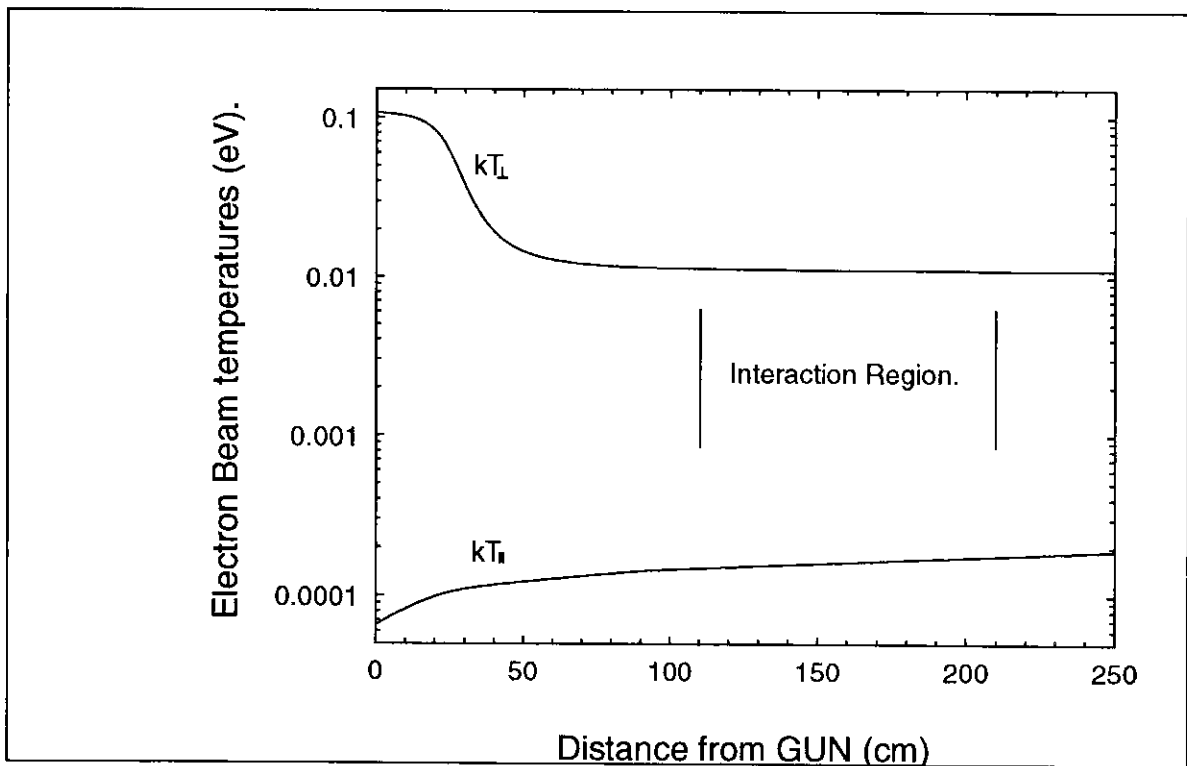


Figure 3.6 *The calculated electron beam temperatures for ASTRID with factor 10 adiabatic expansion.*

mined from the experimental spectra of dielectronic recombination. When a narrow isolated DR resonance is considered, it can be assumed that $\sigma(v)$ is just a δ function. In this case, the integral in eq.(3.5), with f given by eq.(3.6) can be solved analytically in the neighborhood of the resonance, giving $\langle v\sigma \rangle$ as a function of the detuning Δ or, equivalently, as a function of $E_{rel,0}=m\Delta^2/2$

$$\begin{aligned} \langle v\sigma \rangle(E_{rel,0}) = & \text{constant} \cdot \exp\left(-\frac{E_{rel,0}}{kT_{\parallel}} - \frac{E_{res}}{kT_{\perp}} + \frac{E_{rel,0}}{kT_{\parallel}(1-kT_{\parallel}/kT_{\perp})}\right) \\ & \cdot \left[\text{erf}\left(\left|\sqrt{\frac{E_{res}}{kT_{\parallel}}(1-kT_{\parallel}/kT_{\perp})} - \sqrt{\frac{E_{rel,0}}{kT_{\parallel}(1-kT_{\parallel}/kT_{\perp})}}\right|\right) \right. \\ & \left. - \text{erf}\left(\sqrt{\frac{E_{res}}{kT_{\parallel}}(1-kT_{\parallel}/kT_{\perp})} + \sqrt{\frac{E_{rel,0}}{kT_{\parallel}(1-kT_{\parallel}/kT_{\perp})}}\right) \right] \end{aligned} \quad (3.21)$$

where E_{res} is the resonance energy, and erf is the error function defined as

$$\text{erf}(x) = \frac{2}{\sqrt{\pi}} \int_0^x e^{-u^2} du. \quad (3.22)$$

The parameters E_{res} , constant, kT_{\perp} , and kT_{\parallel} can then be varied to obtain the best fit to the data points. Figure 3.7 shows such a fit for the electron beam used in the tandem accelerator experiments. The resonance was $O^{6+}(1s2s^1S) + e^- \rightarrow O^{5+}(1s2p(^1P)11D)$, and the result of the fit was $kT_{\parallel}=10(5) \cdot 10^{-4} \text{eV}$ and $kT_{\perp}=0.135(10) \text{eV}$. In fig.3.8 is shown the corresponding electron-beam-temperature determination for the Heidelberg electron beam performed with a C^{4+} beam. We used the

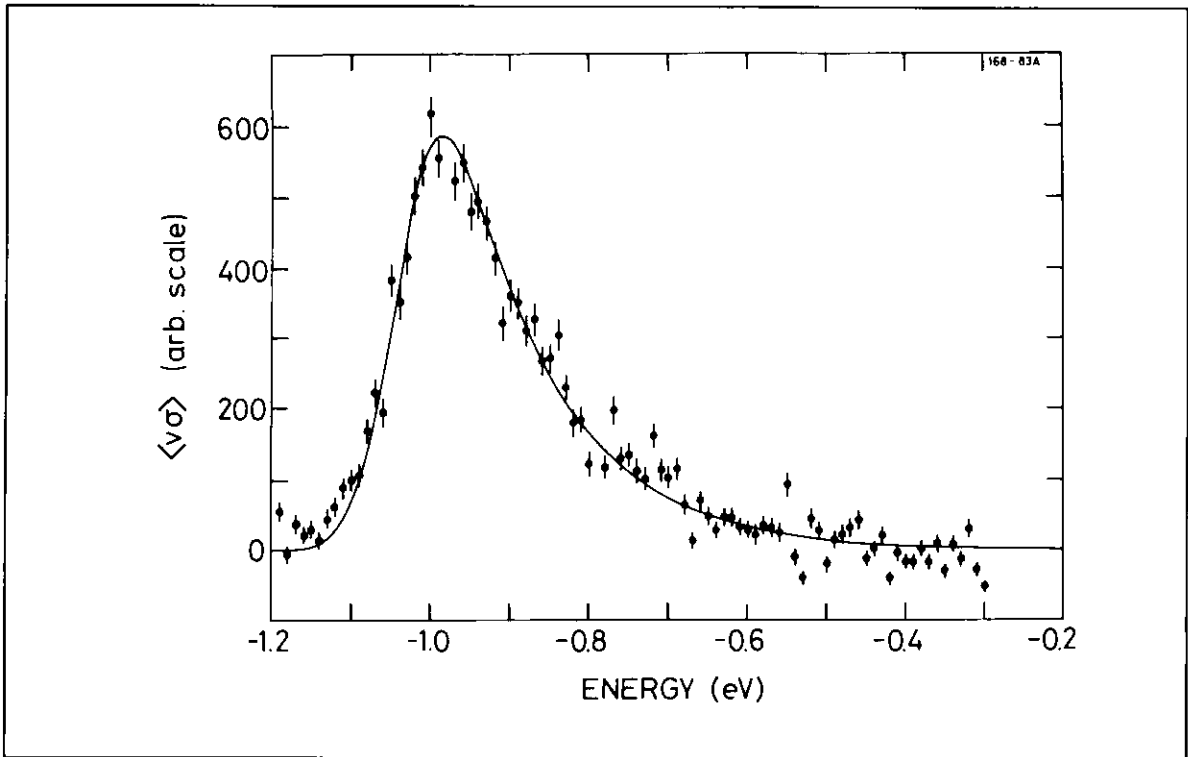


Figure 3.7 *Data points and fit function at the resonance used for the tandem temperature fit. (The negative energy sign just means that the electrons moved slower than the ions).*

resonance $C^{4+}(1s2s\ ^3S) + e^- \rightarrow C^{3+}(1s2s(^1P)7l)$ and found the temperatures $kT_{\parallel} = 6.3(5) \cdot 10^{-4} \text{ eV}$ and $kT_{\perp} = 0.134(10) \text{ eV}$. Due to the larger l splitting for this resonance, a fit was made to *two* δ -shaped resonances. Furthermore, a first-order polynomial was introduced to take into account a slope in the 'background recombination' signal probably caused by the next resonance in the spectrum.

When comparing the measured temperatures for the tandem experiments with the calculated ones, we find reasonable agreement. The slightly higher value for kT_{\perp} can be ascribed to non-uniformity of the solenoid field, but also the ion-beam divergence plays a role since different ions will have slightly different angles with respect to the electron beam, thereby contributing to the spread of relative transverse velocities. Concerning kT_{\parallel} , the effect of the finite size of the ion beam

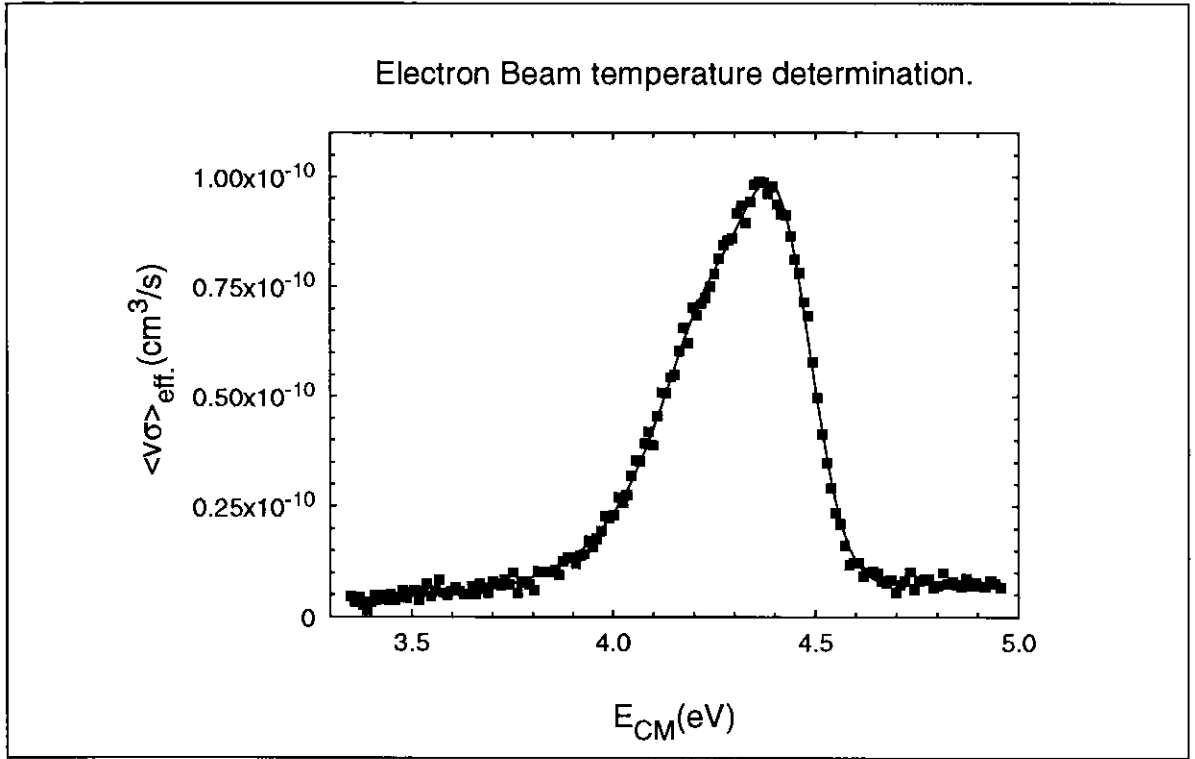


Figure 3.8 *Electron-beam-temperature determination for the TSR electron beam using a C^{4+} beam.*

comes into play since different transverse positions correspond to different values of the electron-beam space-charge potential given by

$$V_{\text{sp}} = \frac{I(\text{A})}{\sqrt{E_0(\text{eV})}} \cdot 1.5 \cdot 10^4 \left[\left(\frac{r}{a} \right)^2 - 1 + 2 \ln \left(\frac{a}{R} \right) \right], \quad (3.23)$$

where a is the electron-beam diameter and R is the diameter of the vacuum chamber. A 1 mm ion-beam radius combined with a 1 mm displacement can then give about 1 V variation in electron space charge across the ion beam for a 10 mA, 1 keV electron beam. This is equivalent to an increase in the peak-to-peak ripple on the acceleration voltage of 1 V. Inserting this in the calculations presented above leads to an increase of almost 50% in kT_{\parallel} . Finally, it is important to bear in mind that electron-beam temperatures measured

with this technique will always be upper limits since any effects of 'non- δ likeness' (e.g finite energy width or l splitting) will lead to apparently higher beam temperatures.

3.3. Electron cooling

Let us consider the electron beam as seen from a reference frame moving with the average electron velocity. If an ion enters this free electron plasma from any direction, it will experience a friction force directed opposite to its velocity vector. The force is known as the drag force and is caused by large-impact-parameter Rutherford scattering between the ions and the electrons. In the single-pass experiments, the influence of the drag force on the recombination experiments could be neglected, but in the storage ring, where the ions pass through the electron cooler several hundred thousand times per second, the accumulated effects of all these passages may be quite significant. In this section, the effects of the drag force relevant to the ion-electron recombination experiments will be discussed qualitatively, and results of cooling of a 4 MeV D^+ beam in ASTRID will be presented.

When the ions and electrons are tuned to the same average velocity, the slower ions are accelerated, and the faster ones are decelerated, leading to a narrowing of the longitudinal velocity distribution of the ions. This is known as longitudinal electron cooling. The process is especially interesting when the initial temperature of the ion beam is so high that the assumption we made in the previous section, that the relative velocity distribution can be well approximated

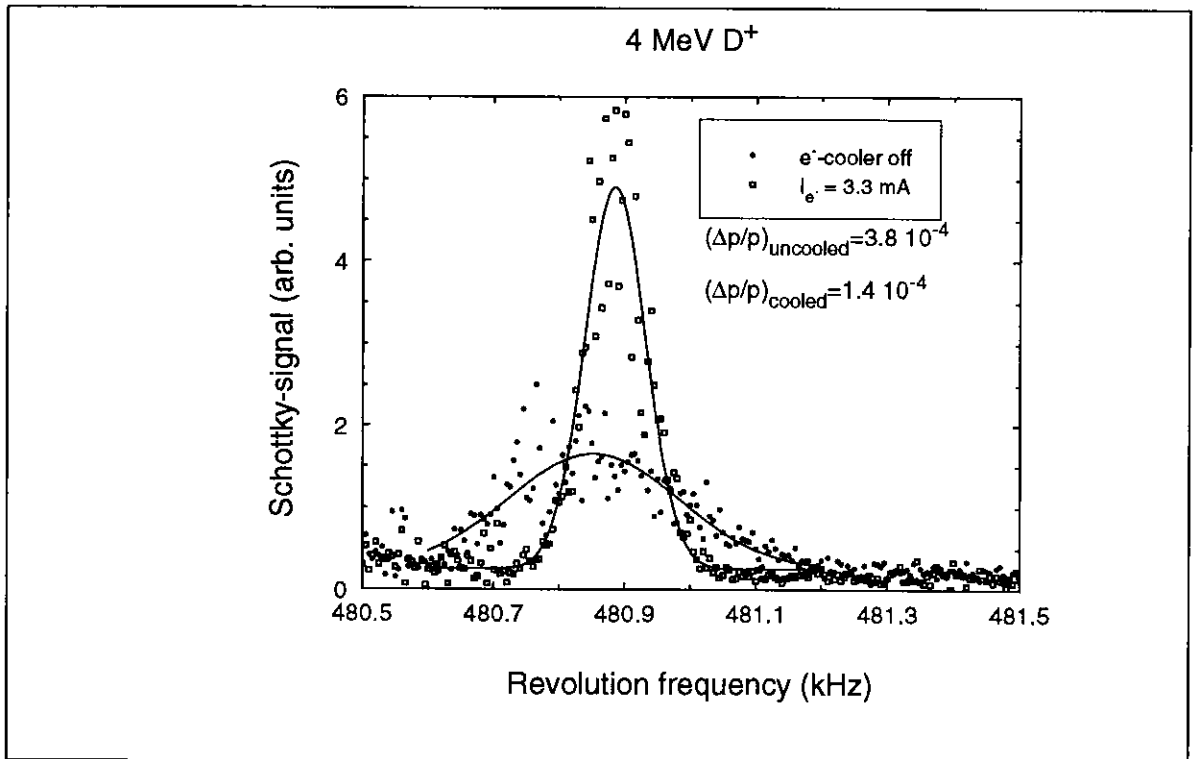


Figure 3.9 Schottky-noise spectra with gaussian fits of a 4 MeV D^+ beam stored in ASTRID. The squares show the cooled beam, and the dots show the uncooled ion beam.

by the electron velocity distribution, no longer holds. In this situation, electron cooling of the ions can practically eliminate the influence from the ion-beam velocity distribution. In fig. 3.9 is shown the Schottky-noise spectrum of a 4 MeV D^+ beam with (squares) and without (dots) electron cooling. This spectrum is the power spectrum of the electrostatic pick-up signal from a cylindrical electrode through which the ion beam passes. Any density fluctuations in the ion beam give rise to a signal at the revolution frequency and its harmonics. The Schottky-noise spectrum hence gives the distribution of revolution frequencies of the ions. To deduce the relative momentum spread from the relative frequency spread, one must divide by the off-momentum factor given by (Poth 1990),

$$\eta = 1 - (v/c)^2 - \alpha, \quad (3.24)$$

where the momentum compaction factor α is defined as

$$\alpha = \frac{\Delta C/C}{\Delta p/p}, \quad (3.25)$$

where C is the circumference of the orbit of a particle with momentum p . For standard ASTRID operation, $\alpha = 0.053$ (Møller 1994), leading to $\eta = 0.943$ for a 4 MeV D^+ beam. For the cooled beam from fig.3.9, we found $\Delta p/p = 1.44 \cdot 10^{-4}$, where Δp is defined as the standard deviation from the mean value of p . Introducing a 'temperature' in analogy to the electron-beam case, we find $kT_{\text{ion}} = 82$ meV, which is much higher than the expected longitudinal *electron* beam temperature of about 1 meV. We see that we do not get complete temperature equilibration between the ions and the electrons. The heating mechanism responsible for this difference is the intra-beam scattering of the ion beam. In the case of equilibrium between intra-beam scattering and electron cooling, $\Delta p/p$ is proportional to $N_i^{0.4}$, where N_i is the number of stored ions (Poth 1990). In table 3.3 is shown $\Delta p/p$ for three different ion intensities, and we see that the $N_i^{0.4}$ dependence is confirmed.

When there is a detuning of the two beam velocities, the drag force will have the same direction for all ions, leading to acceleration or deceleration of the entire ion beam. This can be an obstacle for measuring recombination rate coefficients at very low relative energies, where the drag force is at maximum. This problem is normally circumvented by modulating the electron energy between cooling energy (zero detuning) and the energy at which one wants to measure.

Table 3.3

Ion current $I_i(\mu\text{A})^*$	$\Delta p/p$	$\Delta p/p \cdot (I_i(\mu\text{A}))^{-0.4}$
5	$1.7 \cdot 10^{-4}$	$8.9 \cdot 10^{-5}$
1	$6.9 \cdot 10^{-5}$	$6.9 \cdot 10^{-5}$
0.5	$5.5 \cdot 10^{-5}$	$7.3 \cdot 10^{-5}$

*) *The absolute value of the ion current is only known within a factor of two, but by monitoring the production of neutrals, a relative current measurement with an uncertainty of about 2% could be performed.*

We measured the drag force as a function of the detuning by setting a certain detuning and then watching the drift of the peak in the Schottky spectrum as a function of time. The result of this is shown in

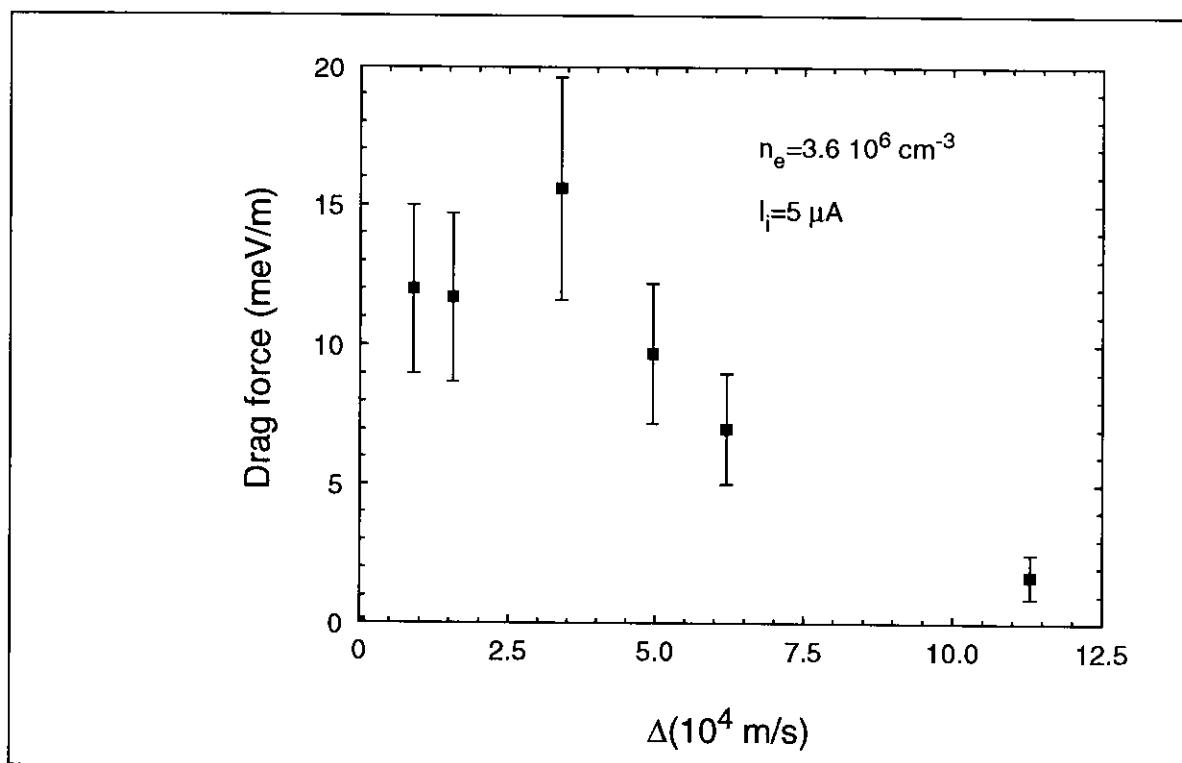


Figure 3.10 *The measured drag force as a function of the detuning velocity Δ .*

fig.3.10.

So far, we have considered only effects of the drag force in the longitudinal direction, but a damping of the transverse motion also takes place. This damping leads to lower transverse ion-beam temperature, smaller beam size, and elimination of the loss of stored particles due to multiple scattering in the residual gas. This last point is illustrated in fig.3.11, where we see that the storage lifetime of a D^+ beam is increased by more than one order of magnitude by applying electron cooling.

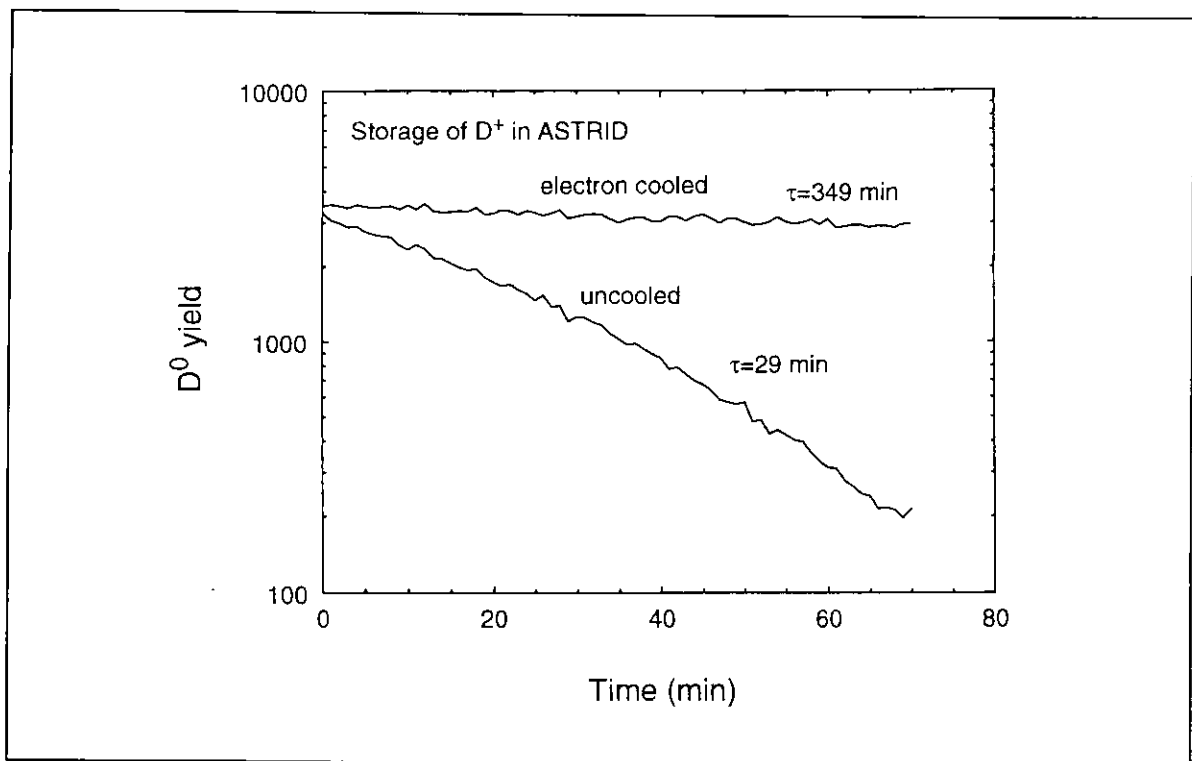


Figure 3.11 Yield of neutrals from stored D^+ beam as a function of time after injection. The upper curve was obtained by applying electron cooling ($n_e=3.6 \cdot 10^6 \text{ cm}^{-3}$).

H Danared (1993) Nucl.Instr&Methods A335 397

N S Dikansky et al.(1987) Proc. XIII Intern. Conf. on High Energy Accel.- Nauka I 330.

D C Griffin (1989) Physica Scripta T28 17

D Habs, J Kramp, P Krause, K Matl, R Neumann, and D Schwalm (1988) Physica Scripta T22, 269

W Hermansfeldt, SLAC report 226 (Stanford 1979).

V I Kudelainen, V A Lebedev, I N Meshkov, V Parkhomochuk, and B N Sukhina (1982) Sov.Phys.JETP 56 1191.

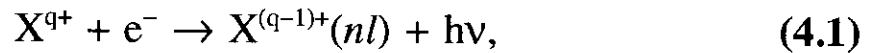
S P Møller (1994) Private communication.

H Poth (1990) Physics Reports 196 135.

4. Radiative Recombination

In this chapter, the process of radiative recombination (RR) is being discussed, and results of the tandem accelerator single-pass experiments are presented. Section 4.1 on RR for fully stripped ions serves as an introduction to the two following sections on RR for non-fully stripped ions (sec.4.2) and on laser-induced recombination (sec.4.3).

The formal prescription of RR is



where q is the ion charge in units of the elementary charge e , n and l are the principal and orbital angular momentum quantum numbers of the captured electron, respectively, and $h\nu$ is the energy of the photon emitted.

4.1 RR for fully stripped ions

We start by considering the case of the initial-state ion being a bare nucleus. For this case, an approximative calculation of the RR cross section was performed by Kramers (Kramers 1923). The Kramers formula gives the cross section for capture to a final state with principal quantum number n ,

$$\sigma_n = 2.10 \cdot 10^{-22} \text{cm}^2 \cdot \frac{Z^4 (e^2 / (2a_0))^2}{n E_{\text{rel}} (Z^2 (e^2 / (2a_0)) + n^2 E_{\text{rel}})}, \quad (4.2)$$

where Z is the nuclear charge in units of e , and a_0 is the Bohr radius.

The derivation of this formula is based on the old quantum mechanics of Bohr and Sommerfeld. The idea is to consider the classical wavelength distribution of the light emitted from an initially free electron, accelerated in the Coulomb field of the nucleus. This wavelength distribution is then modified to take into account the discrete energy levels of the final state, as well as the quantization of light introduced through Einstein's formula,

$$E_{\text{photon}} = h\nu = hc/\lambda. \quad (4.3)$$

With these restrictions, the continuous classical distribution is modified to a series of discrete values. In accordance with the correspondence principle, it is assumed that the integral of the energy emitted in the form of light would be the same as found in the classical calculation. With this assumption, the light emitted in a certain wavelength interval in the classical calculation, can now be associated with radiative recombination into a bound state with a certain principal quantum number n . This procedure leads to the Kramers formula.

After the development of the modern quantum mechanics, exact calculations of the RR cross section for fully stripped ions were performed (Stobbe 1930). These give rise to corrections to the Kramers formula described via the so-called 'Gaunt factors' g_{nl} (Gaunt 1930), defined as the exact cross section divided by the cross section given by the Kramers formula. The l -averaged Gaunt factors may be expressed

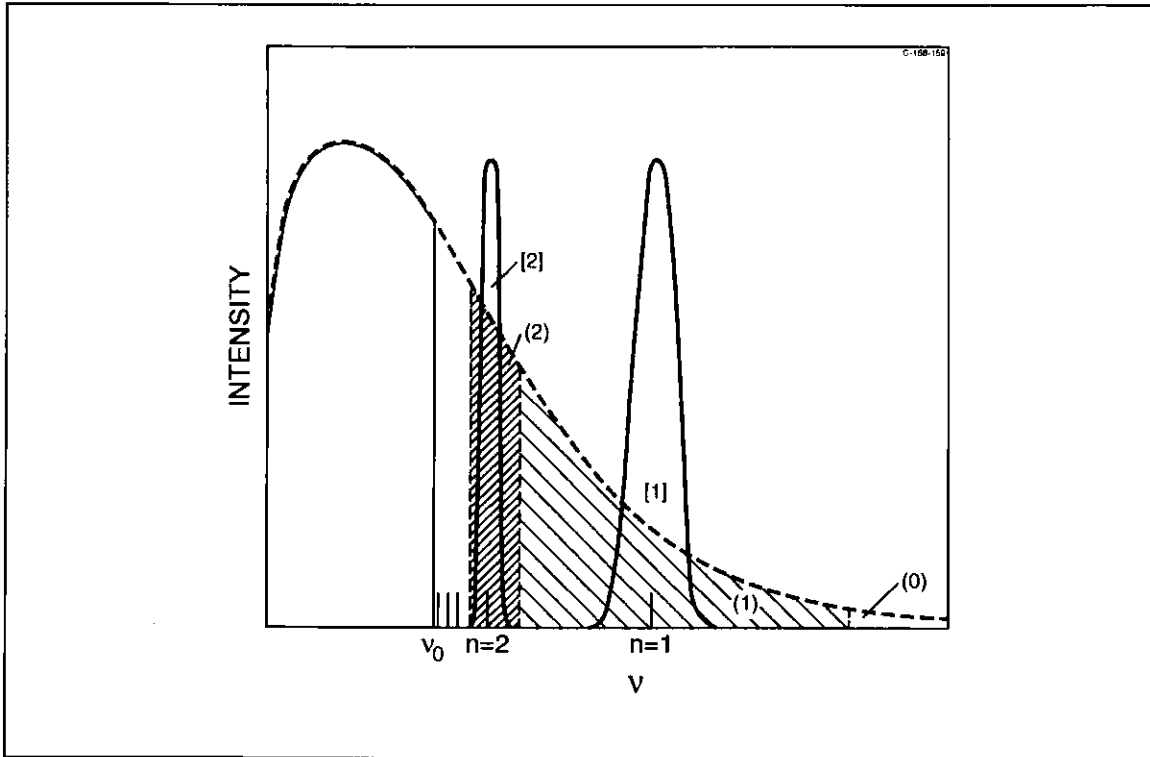


Figure 4.1 *Illustration of Kramers's discretization principle of the emitted radiation.*

by the following asymptotic expansion (Seaton 1959, Griffin 1989):

$$\begin{aligned} \bar{g}_n = & 1 + 0.1728n^{-2/3}(u+1)^{-2/3}(u-1) \\ & - 0.0496n^{-4/3}(u+1)^{-4/3}(u^2+(4/3)u+1) + \dots, \end{aligned} \quad (4.4)$$

where $u = E_{\text{rel}} / (h\nu - E_{\text{rel}})$.

From the quantum mechanical point of view, RR is a radiative transition from a continuum state to a bound state described by the following transition matrix element:

$$T_{fi} = \langle \varphi_{nl}, \bar{k}\rho | H_{\text{int}} | \psi_{\bar{k}}^+, \text{vac} \rangle, \quad (4.5)$$

where the final state is a bound state, φ_{nl} , of the H-like ion plus a photon with wave vector \bar{k} and polarization $\bar{e}_{\bar{k}\rho}$. The initial state is a 'free' electron (distorted by the infinite-ranging Coulomb potential) and

the vacuum state of the electromagnetic field. The interaction Hamiltonian takes on the form (Weissbluth 1978)

$$H_{\text{int}} = -\frac{e}{mc} \cdot \bar{\mathbf{e}}_{\mathbf{k}\rho} \cdot \bar{\mathbf{p}} \left(a_{\mathbf{k}\rho} e^{i\mathbf{k}\cdot\bar{\mathbf{r}}} + a_{\mathbf{k}\rho}^+ e^{-i\mathbf{k}\cdot\bar{\mathbf{r}}} \right), \quad (4.6)$$

where $a_{\mathbf{k}\rho}$ and $a_{\mathbf{k}\rho}^+$ are the photon annihilation and creation operators, respectively. For radiative recombination, only the creation operator yields non-zero matrix elements. For photoionization, which is the inverse process, only the annihilation operator contributes.

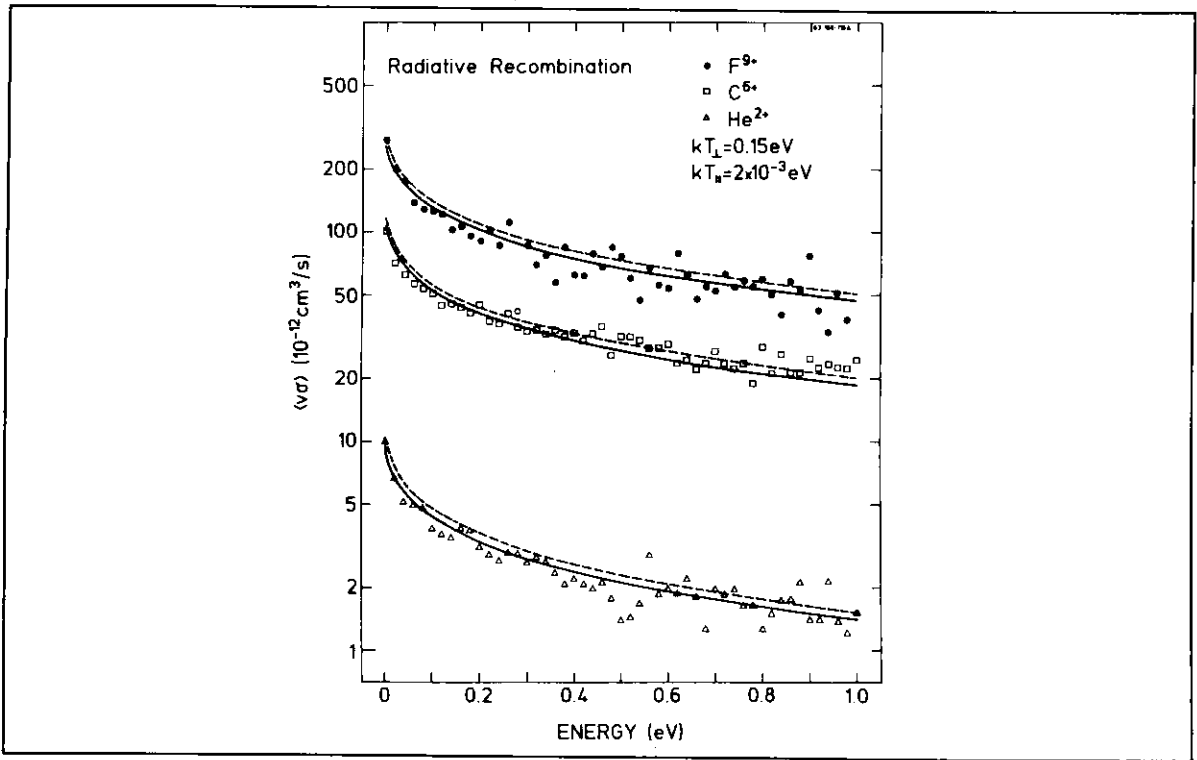


Figure 4.2 RR rate coefficient as a function of relative energy for He^{2+} , C^{6+} , and F^{9+} . Kramers's result with (full curve) and without (dashed curve) Gaunt corrections (Andersen 1990a).

A detailed derivation of the cross section as a function of the relative energy from evaluation of the matrix elements of eq.(4.5) is presented in the thesis of Jakob Bolko (Bolko 1991).

Measurements of RR for He^{2+} , C^{6+} , and F^{9+} in the Aarhus single-pass tandem experiment (Andersen 1990a) confirm these calculations (see fig.4.2) when the effect of field ionization caused by the electric charge-state analyzer field is taken into account. Other experimental studies, performed at the Test Storage Ring (TSR) at the Max Planck Institute Heidelberg, indicate discrepancies of up to 50% for C^{6+} and Cl^{17+} (Wolf 1991), the measured rate coefficient being larger than the theoretically predicted value.

4.2 RR for non-fully stripped ions

For non-fully stripped ions, calculations become more complicated since the final state is no longer a hydrogenic one. However, for states with relatively high n quantum number, the dominating contribution to RR comes from states with $l \geq 2$, and the hydrogenic approximation may be applicable. Since the decrease in the cross section with increasing n given by the Kramers formula is slow for relative energies close to zero, the total cross section will be dominated by contributions from states for which the hydrogenic approximation is good. It is therefore reasonable to use the hydrogenic approximation for the total radiative recombination cross section $\sum_n^{\text{limit}} \sigma_n$, where the summation is restricted to non-occupied levels. It is, however, not clear which charge should be entered in the Kramers formula for this situation. Electrons with high angular momentum will not penetrate the core, and one will expect the effective charge that one should use to be equal to the ion charge. For low- l electrons, however, the incoming electron may penetrate the ion core, leading to an effective charge

higher than the ion charge q and smaller than the nuclear charge Z . A theoretical discussion of the nl dependence of the effective charge derived from Hartree-Fock calculations is given by McLaughlin and Hahn (MacLaughlin 1991), Sunggi and Lin (Sunggi 1991), and Kim and Pratt (Kim 1983). In our measurements, no information on the final state of the recombination products was available. We could, however, deduce an average effective charge q_{eff} by comparing our data to the result of hydrogenic calculations with different values of the charge inserted in the Kramers formula. With this procedure, good agreement with experiments has been found for the H-like ions C^{5+} , O^{7+} , and F^{8+} , as well as for Li-like O^{5+} and Si^{11+} , in all cases using $q_{\text{eff}}=q$ (Andersen 1990b),[II]).

Figure 4.3 shows the result of our measurement of the RR rate coefficient for the O-like Si^{6+} ion [II]. Also shown in this figure are the results of the hydrogenic approximation using $q_{\text{eff}}=q=6$ and $q_{\text{eff}}=9$, respectively. We see that in order to reproduce our experimental data, $q_{\text{eff}}=9$ should be used. The fact that $q_{\text{eff}}>q$ we take as evidence of incomplete screening. For F^{3+} [V], we also observed incomplete screening.

Since it has been found that for H-like and Li-like ions, one should use $q_{\text{eff}}=q$, whereas for C-like and O-like ions $q_{\text{eff}}>q$, it is tempting to ascribe the effect of incomplete screening to the presence of 2p electrons in the initial-state ion. This observation is probably related to the fact that p-wave functions extend to larger distances from the nucleus than s-wave functions.

Another measurement of RR for non-fully stripped ions was performed by Müller et al. on U^{28+} ions (Müller 1991). They found a maximum rate coefficient of $r \approx 1 \cdot 10^{-7} \text{cm}^3 \text{s}^{-1}$. This was compared to a

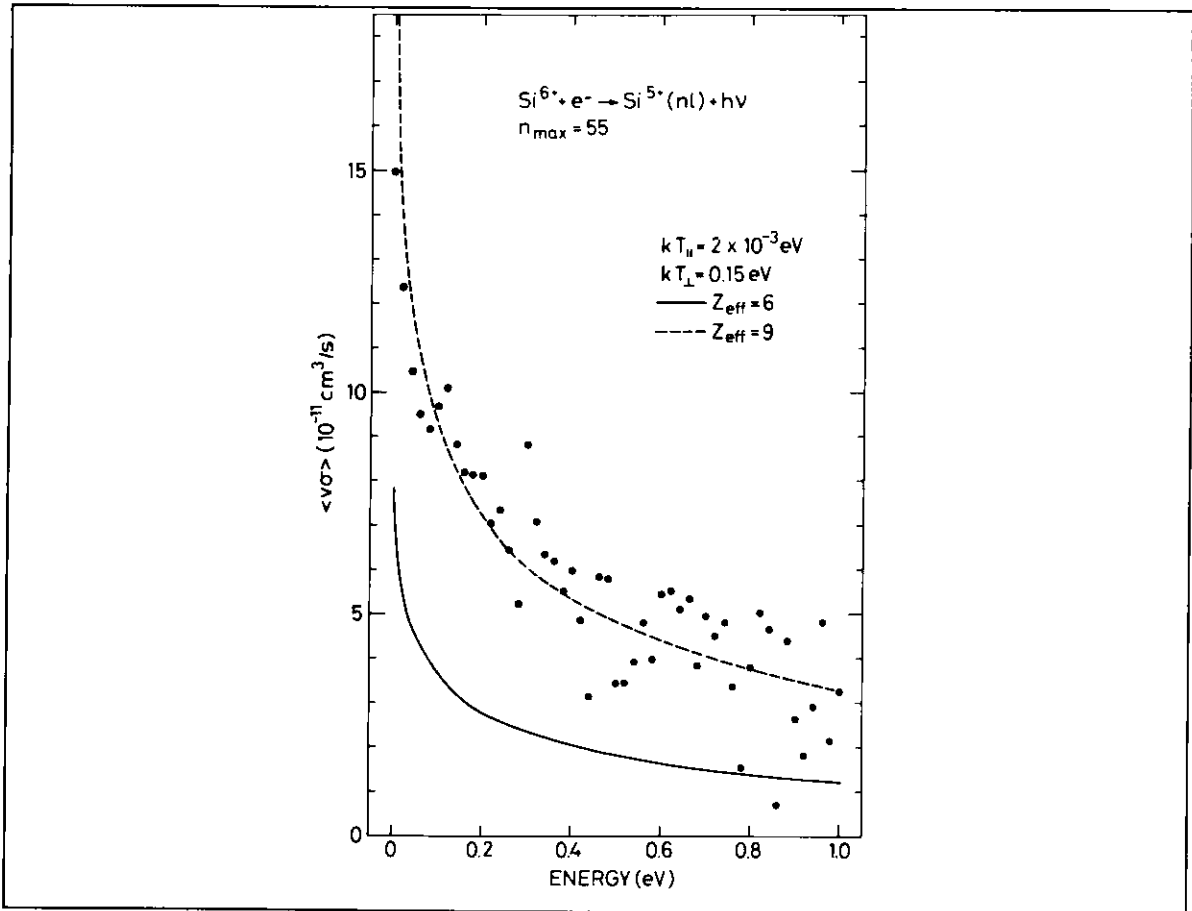


Figure 4.3 *The measured RR rate coefficient for Si^{6+} compared to theoretical values obtained with two different effective charges.*

hydrogenic calculation using $q_{\text{eff}}=60$, and it was found that the experimental result exceeded theory by a factor of five.

We note that since for relative energies close to zero energy, $\sigma_{\text{RR}} \propto Z_{\text{eff}}^2$, the result of Müller et al. would exceed theory by a factor of two, even if they used $q_{\text{eff}}=Z=92$, corresponding to no screening by the 64 electrons on the ion. It is therefore probable that what they saw was not only RR. Some other mechanism must have contributed. One possibility is some DR resonance very close to 0 eV. Another possibility is ternary recombination (see ch.2) since they had very high electron densities, of the order of 10^{10} cm^{-3} . This should be compared to the electron density in our single-pass experiment which was

typically about $5 \cdot 10^7 \text{ cm}^{-3}$.

4.3 Laser-induced RR

In sec.4.1, we considered matrix elements of the form

$$T_{fi} = \langle \varphi_{nl}, \bar{k}\rho | H_{int} | \psi_{\bar{k}}^+, \text{vac} \rangle. \quad (4.7)$$

We now let N denote the number of photons with wave vector \bar{k} and polarization $\bar{e}_{\bar{k}\rho}$ and consider the following matrix element:

$$T_{fi} = \langle \varphi_{nl}, (N+1) | H_{int} | \psi_{\bar{k}}^+, N \rangle. \quad (4.8)$$

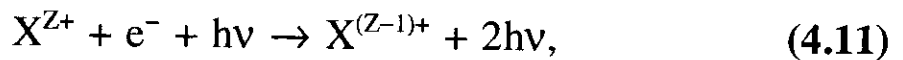
It is a property of the creation operator mentioned in sec.4.1 that

$$a_{\bar{k}\rho}^+ |N\rangle = \sqrt{N+1} |N+1\rangle. \quad (4.9)$$

This leads to

$$|T_{fi}|^2 \propto (N+1). \quad (4.10)$$

In other words, with a laser field of the proper frequency, radiative recombination can be stimulated via the following reaction:



where the two photons in the final state are identical. This possibility was considered by Neumann et al. (Neumann 1983).

If we consider initial-state ions that are fully stripped, the energy

conservation implies

$$h\nu = \frac{1}{2}mv_{\text{rel}}^2 + \frac{Z^2 e^2}{n^2 2a_0} . \quad (4.12)$$

We now let $\Delta\nu$ denote the combined spectral width of the laser field and the n 'th energy level. The stimulated process will then be possible for electrons in the velocity interval $v_{\text{rel}} \pm \Delta v_{\text{rel}}$, where $\Delta v_{\text{rel}} = \frac{h\Delta\nu}{mv_{\text{rel}}}$.

The gain is defined as

$$g_n = \frac{r_n^{\text{IND}}(\Delta v_{\text{rel}})}{r_n^{\text{SPON}}(\Delta v_{\text{rel}})} , \quad (4.13)$$

where $r_n^{\text{IND}}(\Delta v_{\text{rel}})$ and $r_n^{\text{SPON}}(\Delta v_{\text{rel}})$ denote the rates for induced and spontaneous recombination to the state n for electrons in the velocity interval $v_{\text{rel}} \pm \Delta v_{\text{rel}}/2$, respectively. The gain can be determined using Einstein's A and B coefficients. The result is

$$g_n = \frac{Ic^2}{8\pi h\nu^3 \Delta\nu} , \quad (4.14)$$

where I is the laser intensity.

The quantity g_n , however, is not what is measured directly as long as only charge state analysis is used. What influences the measured recombination rate is the total gain G_n defined as

$$G_n = \frac{r_n^{\text{IND}}(\Delta v_{\text{rel}})}{r^{\text{SPON}}} = g_n \frac{r_n^{\text{SPON}}(\Delta v_{\text{rel}})}{r^{\text{SPON}}} , \quad (4.15)$$

where r^{SPON} is the summed rate for all values of n , integrated over the

entire velocity distribution.

r_n^{SPON} can be determined using the Kramers formula and the known velocity distribution. $r_n^{\text{SPON}}(\Delta v_{\text{rel}})$ is determined in the limit $v_{\text{rel}} \rightarrow 0$. Performing these calculations following Neumann et al., leads us to the following expression for G_n at threshold

$$G_n = \frac{1}{n} \frac{4.42 \cdot 10^{-6}}{\sqrt{kT_{\perp}(\text{eV}) kT_{\parallel}(\text{eV})} (h\nu(\text{eV}))^3} I(\text{W/cm}^2). \quad (4.16)$$

For our LIR experiment at the tandem accelerator, we merged a co-propagating beam from a Nd:YAG laser with a He^{2+} beam and an electron beam tuned to zero relative velocity. This laser had a fixed wavelength of $\lambda=1.0641 \mu\text{m}$, corresponding to a photon energy of $h\nu=1.1652 \text{ eV}$. The wavelength in the ion rest frame depended on the Doppler shift, which we could control by varying the beam energies. For an ion energy of 1.07 MeV/amu , the photon energy in the ion rest frame is equal to 1.11 eV , which is equal to the binding energy of an electron in the $n=7$ state of He^+ . By applying a Q switch, the laser could be operated in a pulsed mode giving 3.8 mJ pulses of 200 ns duration, with a repetition rate of 2 kHz . The time-averaged intensity of a laser pulse in the interaction region was 68 kW/cm^2 , leading to an expected total gain of $G_n=2.7$ when the previously found electron-beam temperatures of $kT_{\parallel}=1 \text{ meV}$ and $kT_{\perp}=135 \text{ meV}$ (see sec.3.2) were inserted in eq.(4.15).

The measurement was done by having the laser pulse start a time-to-amplitude converter (TAC) which was stopped by the detection at the channelplate of a He^+ ion. In this way, the production of singly charged He ions could be monitored as a function of time in a narrow time window around the time of the laser pulse. Based on earlier RR

measurements with He^{2+} ions, we could estimate the count rates for spontaneous RR as well as for electron capture in collisions with residual gas molecules, which turned out to be the dominating background signal. From this estimate, we should expect a statistically significant peak in the time spectrum to appear after about 30 minutes of measuring. We did, however, not see any effect of the laser, even after 7 hours. The most important reason for this was probably that we did not have the perfect beam overlap we had assumed in our estimates. Furthermore, it was pointed out by Schramm et al. (Schramm 1991) that weak electric fields in the interaction region can lead to a smearing-out of the threshold, which in turn leads to a reduction of the total gain at threshold by up to a factor of two or three.

After our unsuccessful attempts to make laser-stimulated RR, two other groups have succeeded (Schramm 1991, Yousif 1991). Schramm et al. used merged beams of protons, electrons, and laser light. Their laser system was an excimer-laser-pumped dye laser. ($I \leq 18 \text{ MW/cm}^2$). The final state was $n=2$ in hydrogen. Yousif et al. used merged beams of protons and electrons which were crossed by a cw beam from a CO_2 laser ($\lambda=10.535 \text{ }\mu\text{m}$, $P=15 \text{ W}$). They used a field-ionization technique which made it possible to selectively detect hydrogen atoms formed in states with principal quantum numbers in the range of $8 \leq n \leq 19$. By varying the electron-beam energy, they found an enhancement introduced by the laser for RR to $n=11$ and to $n=12$.

L H Andersen and J Bolko (1990a) Phys.Rev.A 42 1184

L H Andersen and J Bolko (1990b) J.Phys.B. 23 3167

J Bolko (1991) Thesis, Institute of Physics and Astronomy, Aarhus University (Unpublished)

- J A Gaunt (1930) Phil.Trans.A 229 163*
- D C Griffin (1989) Physica Scripta T28 17*
- Y S Kim and R H Pratt (1983) Phys.Rev.A 27 2913*
- H A Kramers (1923) Phil. Mag. 46 836*
- D J McLaughlin and Y Hahn (1991) Phys.Rev. A 43 1313*
- Müller et al (1991) Physica Scripta T37 62*
- R Neumann, H Poth, A Winnacker, A Wolf (1983) Z.Phys.A 313 253*
- M J Seaton (1959) Mon. Not. R. Astron. Soc. 119 81*
- U Schramm, J Berger, M Grieser, D Habs, E Jaeschke, G Kilgus, D Schwalm, A Wolf, R Neumann, R Schuch (1991) Phys.Rev.Lett. 67 22*
- M Stobbe (1930) Ann. Phys. 7 661*
- C Sunggi and C C Lin (1991) Phys.Rev.A 43 3433*
- P Van der Donk, F B Yousif, J B A Mitchell and A P Hickman (1991) Phys.Rev.Lett. 67 42*
- M Weissbluth: Atoms and Molecules (1978) Academic Press*
- A Wolf et al (1991) Z.Phys.D 21 69*

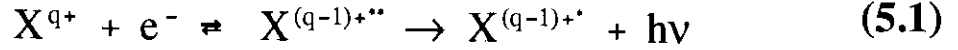
5. Dielectronic Recombination

In this chapter, the process of dielectronic recombination (DR) is being discussed. In particular results from the tandem single-pass experiments on metastable He-like ions [IV], as well as on Li-, Be-, B-, and C-like ions [III, I, V], are considered. Furthermore, previously unpublished results of DR measurements for metastable He-like ions performed at the TSR, MPI-K, Heidelberg are presented.

In sec.5.1 the DR process is introduced, the effects of external electric fields are discussed, and reference is made to other works in the field of DR. Section 5.2 concerns DR for Li-like ions which is a particularly simple case in the sense that no metastable states are involved, and only the 2s-2p excitation is relevant in the energy range considered in these experiments. The remaining sections of this chapter deal with the situation where a fraction of the ions in the beam is formed in electronically excited states which are metastable and hence sufficiently long-lived to be present in the merged-beams experiments. The emphasis will be put on the He-like metastable ions (sec.5.3-4), and in particular on comparisons between the single-pass results [IV] and the results obtained at the TSR.

5.1 Introduction to DR

In the isolated resonance approximation, the DR process is described as a two-step process,

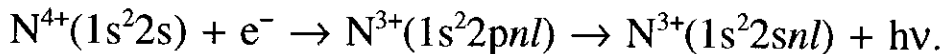


where the doubly excited intermediate state $X^{(q-1)+**}$ in most cases is a Rydberg state with an excited core. The first step will be referred to as the dielectronic capture and has a probability proportional to the autoionization rate A_a of the doubly excited state. The probability for the second step is given as the ratio of the rate for radiative stabilization A_r to the total stabilization rate $A_a + A_r$. The DR cross section is proportional to the product of these two probabilities,

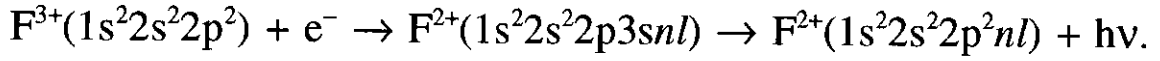
$$\sigma_{nl} \propto \frac{A_a(nl) A_r(nl)}{A_a(nl) + A_r(nl)}, \quad (5.2)$$

where n and l denote the principal and angular-momentum quantum numbers of the captured electron, respectively. After the dielectronic-capture process, the doubly excited state can in general stabilize radiatively or by autoionisation to several different final states. To calculate the DR cross section for a given relative energy, all these rates have to be determined, and eq.(5.2) should therefore only be considered as a formal description.

When discussing DR, one often distinguishes between $\Delta n=0$ and $\Delta n \neq 0$ processes. $\Delta n=0$ denotes a process where the electron, which gets excited as the free electron is resonantly captured, does not change its principal quantum number. As an example of a $\Delta n=0$ process, consider



An example of a $\Delta n \neq 0$ process is

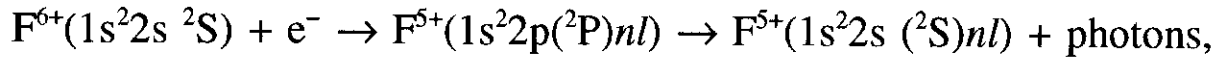


This distinction becomes very important when the effect of external electric fields in the interaction region is considered. The presence of weak electric fields [primarily caused by the electron-beam space charge (see eq.3.23)] in the interaction region is found to dramatically enhance the rate for DR ($\Delta n=0$), whereas only small effects can be found for DR ($\Delta n \neq 0$).

The electric-field enhancement for $\Delta n=0$ processes can be understood qualitatively by the following argument: The radiative stabilization rate is practically independent of the n and l quantum numbers of the captured electron in the doubly excited state since the dominant radiative stabilization (except for the lowest values of n and l) is usually a core stabilization, with the Rydberg electron acting merely as a spectator. The rate for autoionisation, however, is decreasing dramatically when l is increased, so that for low l , $A_a \gg A_r$, while for high l , $A_a \approx 0$ (Griffin 1989). For this reason, only low-to-moderate values of l contribute to the DR cross section.

In the presence of electric fields, the spherical symmetry will be broken, and l is no longer a good quantum number. The physical states will then become linear combinations of states with different l , and all states will have admixtures of low- l states. As a consequence, A_a , and hence the DR cross section, will be increased for states dominated by high- l components as compared to the field-free case, whereas no change is found in the cross section when states dominated by low- l components are considered. For low values of n (typically $n \leq 15$), all possible l states are to be considered low in this context, and therefore field effects are not important. However, for higher n , the field effect

is increasing, so that the contribution from the high Rydberg states can be substantially increased. As an example, we mention that for the following $\Delta n=0$ reaction:



an enhancement of the summed rate coefficient from $n=20$ to $n=58$ by a factor of three to four is found by considering an electric field of 15 V/cm rather than a zero field [III].

For the $\Delta n \neq 0$ transitions, the field effects will be much weaker than for the $\Delta n=0$ transitions. This is due to the fact that for $\Delta n \neq 0$, the value of σ_{nl} will be substantial only for states with relatively low principal quantum numbers n , for which the field effect is known to be insignificant (Griffin 1989). To explain this, we note that the rate A_r is practically independent of n , whereas A_a is approximately proportional to n^{-3} . According to eq.(5.2), this means that there will be a critical principal quantum number n_{crit} for which $\sigma_n = \sum_{l=0}^{n-1} \sigma_{nl}$ is constant if $n < n_{\text{crit}}$ and $\sigma_n \propto n^{-3}$ if $n > n_{\text{crit}}$. For $\Delta n \neq 0$, A_r is in general much larger than for $\Delta n=0$ because of the v^3 dependence in the radiative rate, whereas A_a will be smaller than for $\Delta n=0$ because of the larger energy of the electron in the continuum state. As a consequence, n_{crit} will be much smaller for $\Delta n \neq 0$ transitions than for $\Delta n=0$ transitions, and therefore the high- n states, which have the largest field dependence, will not contribute much to the DR signal (Griffin 1989).

Several DR measurements have been performed using merged beams. The first measurements considered 2s-2p excitations in C^+ ions

(Mitchell 1983). Shortly after this, 2s-2p excitations in Li-like boron and carbon ions were studied (Dittner 1983). With the construction of the Aarhus tandem single-pass experiment, better resolution was achieved, allowing state-selective measurements of DR for He- and Li-like carbon and oxygen ions (Andersen 1990). Since 1990, many experimental results on DR have been published. The most widely used techniques are the merged-beams technique in storage rings (see, e.g., Wolf 1991, Spies 1992) and the electron-beam ion-trap (EBIT) technique (Beiersdorfer 1991, Ali 1991).

The first evidence of the field effect for $\Delta n=0$ processes was reported by Müller et al. (Müller 1987). Crossed beams of ions and electrons were used. The DR process considered was:

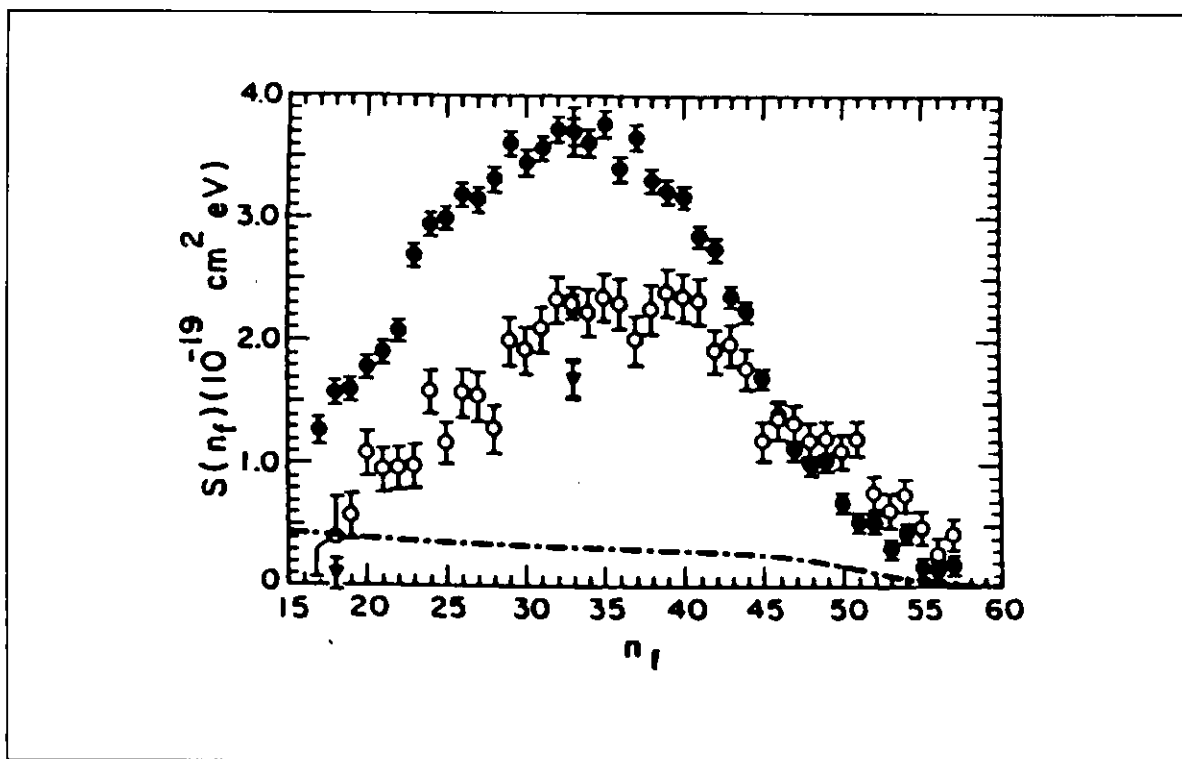
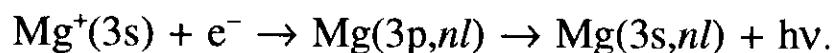
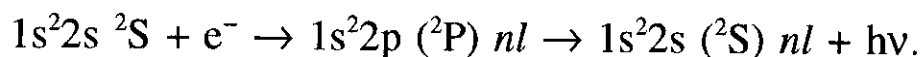


Figure 5.1 Collision strength as a function of the final state n quantum number for fixed relative energy (Müller 1987).

The dominating contribution to the electric field in the interaction region was the motionally induced electric field, caused by the solenoid field, which was applied to confine the electron beam. Müller et al. performed the experiment with two different solenoid fields so that the electric field was 7.2 V/cm and 23.5 V/cm, respectively. For detection, they used a field-ionization technique, so that the final state n could be determined for states with $n \geq 17$. Their result, the yield for constant relative energy as a function of the principal quantum number for the two different field strengths, is shown in fig.5.1 together with a zero-field calculation.

5.2 DR for ground-state Li-like ions

As mentioned in the beginning of this chapter, only one particular electronic excitation is relevant to the DR process for Li-like ions in the low-energy regime, namely the 2s-2p excitation. Therefore the discussion is restricted to DR processes of the following form:



What we expect to see is then a Rydberg series of resonances converging to the 2s-2p excitation energy of the Li-like ion involved. Since this is a $\Delta n=0$ process, we expect a substantial field dependence for the higher- n -states.

In figs.5.2, 5.3, and 5.4 we present our data for N^{4+} , F^{6+} , and Si^{11+} , respectively, together with calculations by Badnell and Pindzola including Stark l -mixing effects for varying electric field strengths

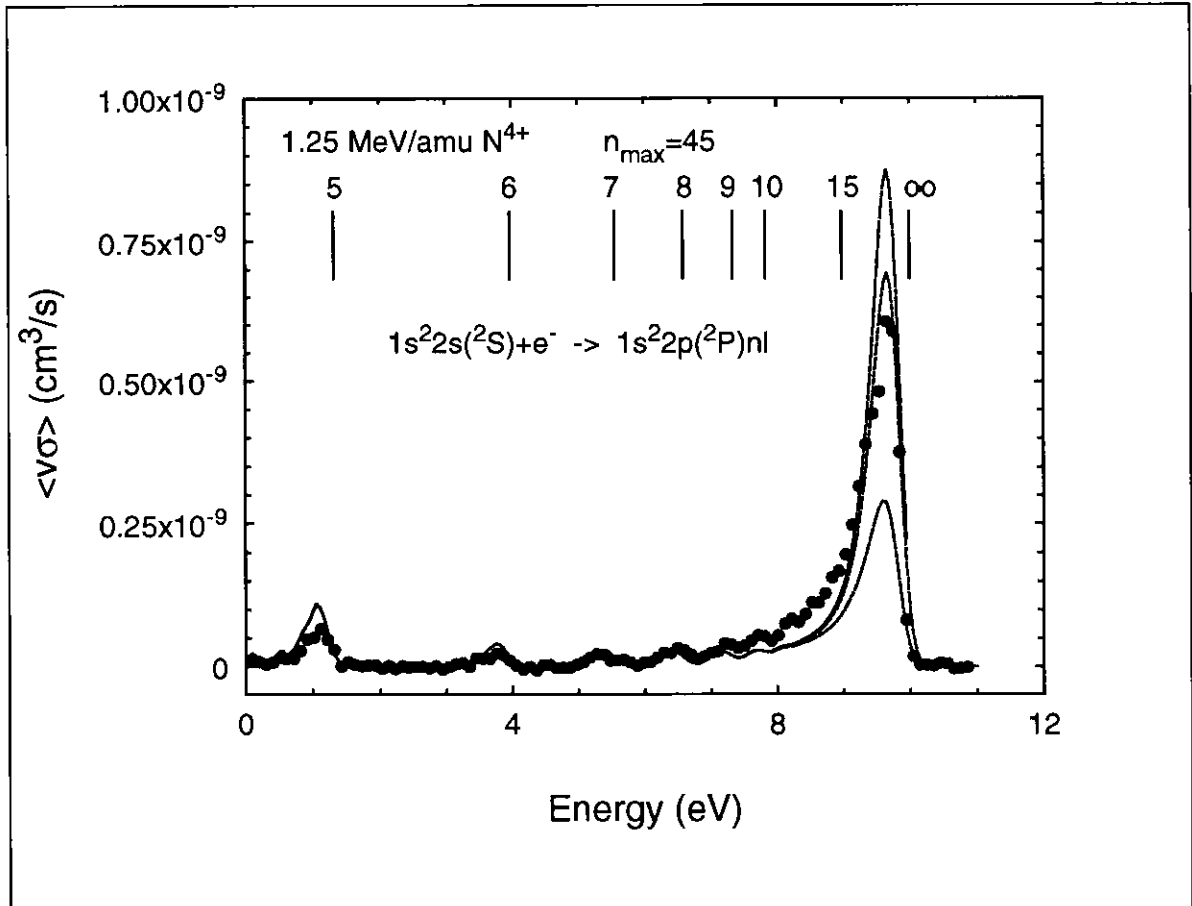


Figure 5.2 Measured and calculated rate coefficients as a function of energy for N^{4+} . The calculations assume electric fields of 0 V/cm, 5 V/cm, and 10 V/cm, respectively.

[III]. The expected resonance positions marked by vertical lines are calculated from the known 2s-2p excitation energy and the assumption that the binding energy of the captured electron is well described by the Rydberg formula without quantum defects. The peaks are always found at a slightly lower energy. This is primarily due to the flattened electron-velocity distribution, as described in sec.3.2, but also non-zero quantum defects for the lowest l values will give a displacement to the low-energy side.

For N^{4+} and F^{6+} , good overall agreement is found. We do, however, notice that theory tends to overestimate the lowest-energy resonances and to underestimate the DR signal for energies just below

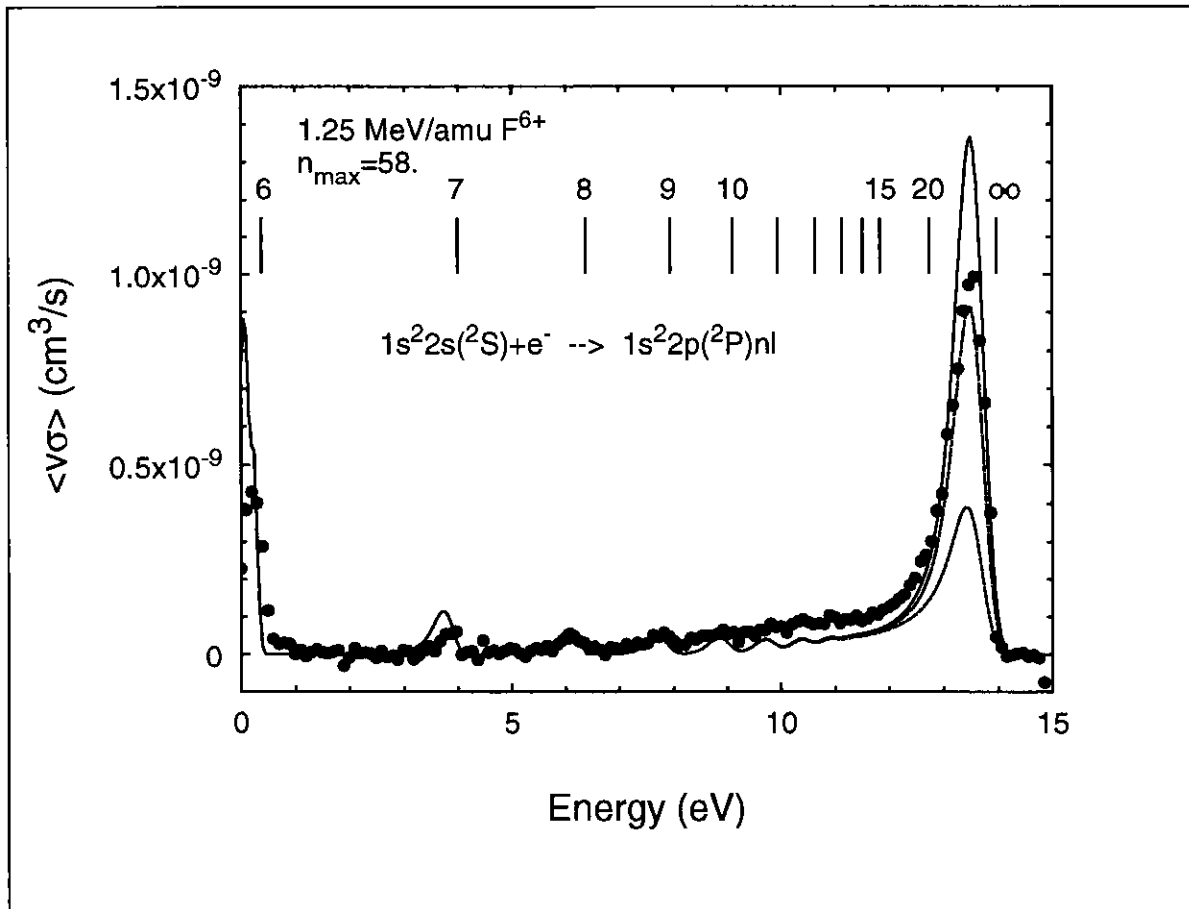


Figure 5.3 Measured and calculated rate coefficients as a function of energy for F^{6+} . The calculations assume electric fields of 0 V/cm, 5 V/cm, and 15 V/cm, respectively.

the Rydberg peaks. The gravest discrepancy appears to be related to the contribution from the $2p6l$ configurations of F^{6+} . These are, however, found to straddle the threshold, making it very difficult to determine which states should be included in the theoretical treatment [III]. It has been proposed (Hahn 1994) that the recombination rate just below the Rydberg peak not accounted for in the DR theory could be due to a 'new' recombination-mechanism; radiative dielectronic recombination, which is a DR process where the initial capture is accompanied by a simultaneous emission of a photon. However, no detailed calculations concerning this contribution have been performed.

For N^{4+} , it seems that the average electric field is a little below

5 V/cm, while for F^{6+} , it seems to be a bit more than 5 V/cm. This agrees with the expected values from the space-charge field and the motionally induced electric field due to small angles between the ion trajectories and the magnetic solenoid field.

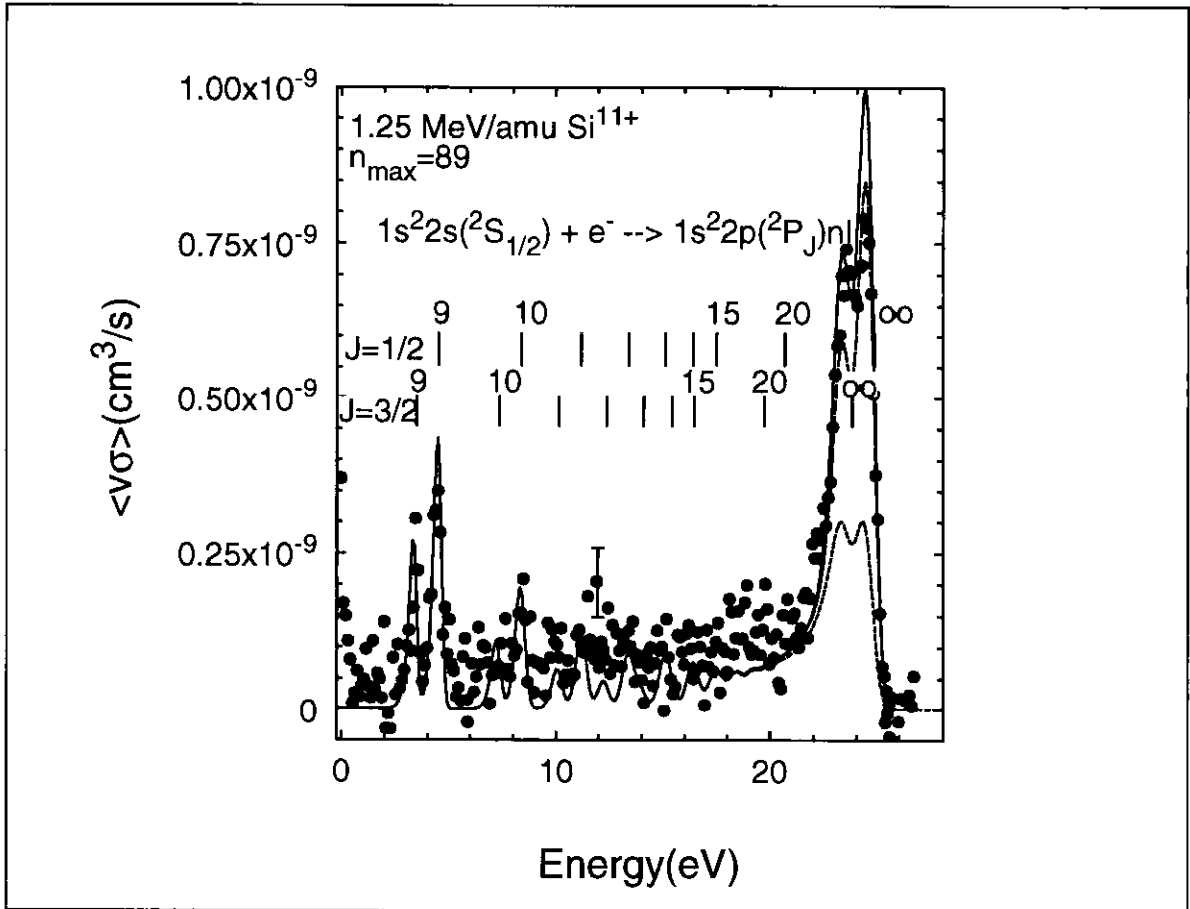


Figure 5.4 Measured and calculated rate coefficients as a function of energy for Si^{11+} . The calculations assume electric fields of 0 V/cm, 5 V/cm, and 10 V/cm, respectively.

For Si^{11+} , the beam current was so low that the statistical errors became rather large. The double structures in this spectrum are due to the fine-structure splitting of the $1s^2 2p \ ^2P$ state (for N^{4+} and F^{6+} , this splitting was too small to be resolved). Considering the double Rydberg peak, the calculations indicate that not only the total rate coefficient, but also the relative height of the two peaks depend on the field strength. If we want to get the relative height right, we must use

an electric field between 0 V/cm and 5 V/cm, but if we want the total recombination rate coefficient to be right, we have to use a somewhat larger field (5-10 V/cm). This discrepancy indicates that either is the electric field dependence not treated correctly in the calculations, or some other mechanism is involved. One mechanism could be radiative stabilization of some of the high Rydberg states before they reach the charge-state analyzer, where they were expected to be field-ionized and therefore not counted as recombined. When discussing the relative height of the two peaks, it should be pointed out that the possibility for the high- n Rydberg levels with a $^2P_{1/2}$ core to autoionize to the $^2P_{3/2}$ continuum has been taken into account in the calculations.

We performed a systematic investigation of the field dependence for N^{4+} . An ion beam was set up and left unchanged, while the integrated DR Rydberg contribution for energies from 8 eV to 10.5 eV was measured. Three different electron currents, corresponding to three different space-charge electric field strengths, were used.

The result of this measurement is shown in fig.5.5. The fields in the experiments were estimated under the assumption that the ion-beam width was $2\sigma=0.2$ cm, and the displacement of the ion beam with respect to the electron beam was between 0 and 0.1 cm. This uncertainty led to the horizontal error bars in the figure. The vertical error bars reflect a 15% uncertainty on the absolute scale. Motionally induced electric fields due to the solenoid magnetic field are not considered. Within the experimental error, agreement with theory is found. We note that this would probably still be the case if the motionally induced field was included since this would on the average displace the experimental points towards higher electric fields.

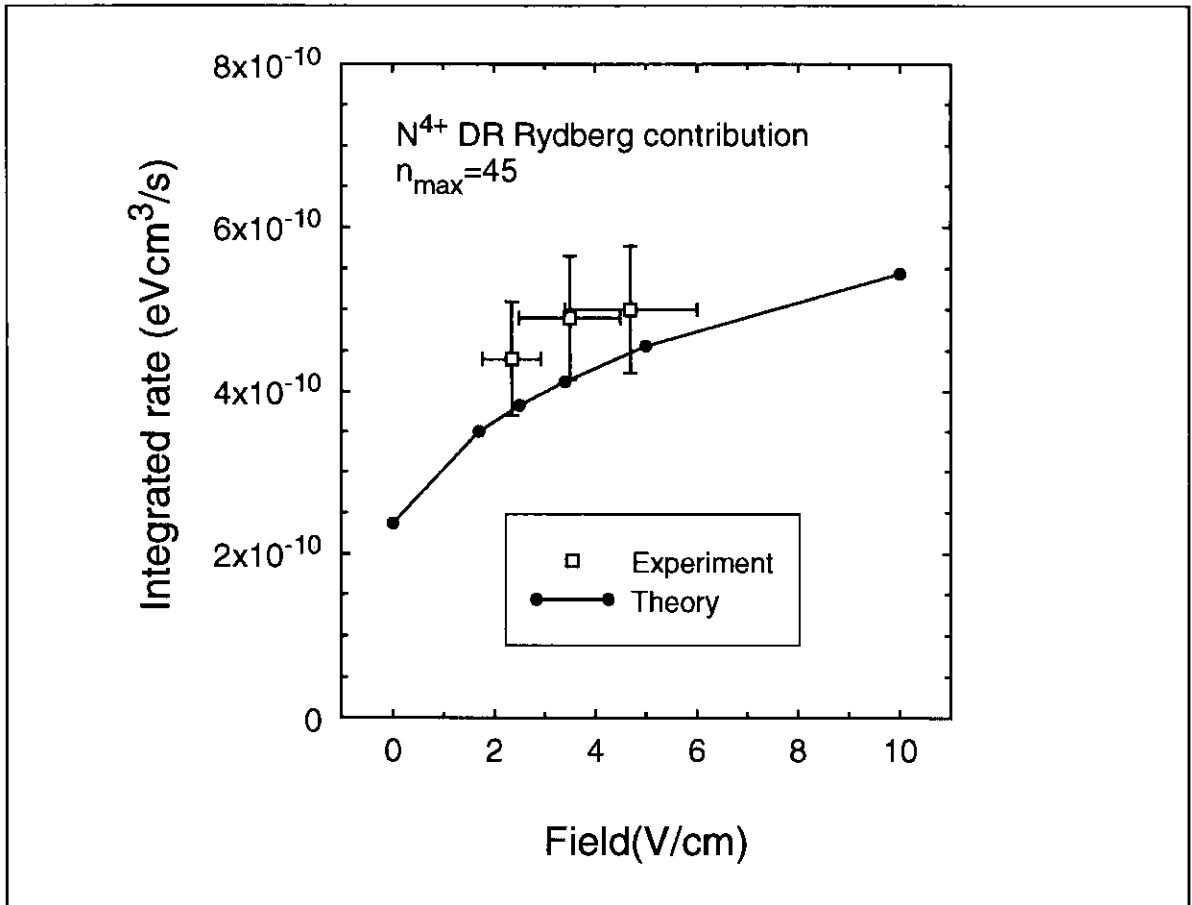


Figure 5.5 *The experimental and theoretical rate coefficient of the high- n contribution for N^{4+} integrated from 8 to 10.5 eV as a function of the calculated space-charge field.*

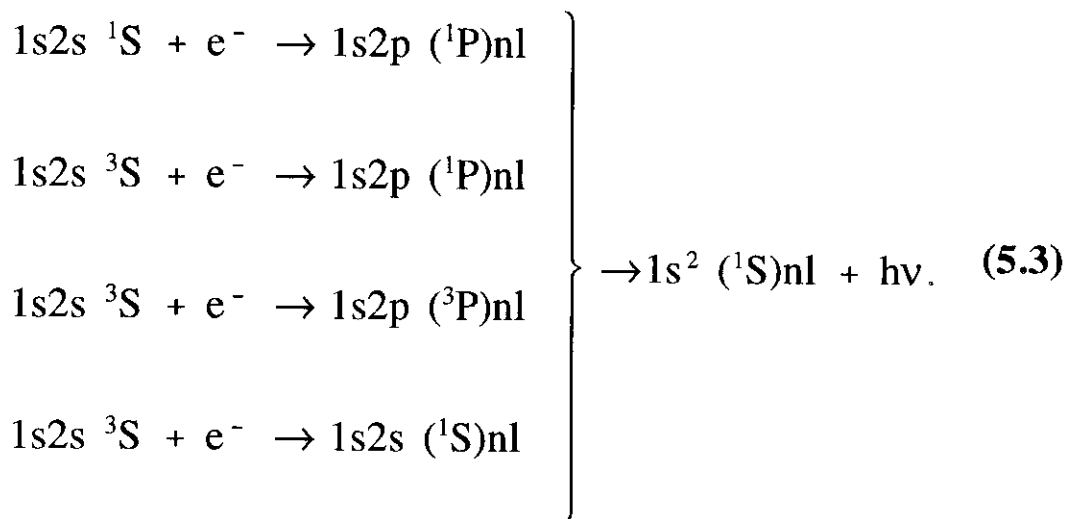
5.3 DR for metastable He-like ions (the single-pass experiment)

In this and the following section, DR for metastable He-like ions is discussed. We start by considering the single-pass experiment and then go on to the Heidelberg storage-ring experiment. The comparison of the two will yield new information concerning the interpretation of the results of the single-pass experiments.

In the single-pass experiment, the He-like ions were produced in a stripping target (gas or foil) placed at the terminal of the tandem

accelerator or, in the case of high nuclear charge, in a stripping target placed right after the tandem accelerator. This production method leads to population of a large number of electronic states. However, most of these states are rather short-lived, so that within a micro-second, all ions are found either in the ground state $1s^2\ ^1S$, or in one of the two metastable states $1s2s\ ^1S$ or $1s2s\ ^3S$. For the ions considered here (N^{5+} , F^{7+} and Si^{12+}), the $1s2s\ ^3S$ states live much longer than the flight time from the place of production to the interaction region (Drake 1971). Hence, contribution from the $1s2s\ ^3S$ -state to the observed recombination spectrum is expected for all these ions. The $1s2s\ ^1S$ lifetimes, on the other hand, are comparable to the flight time (for N^{5+}) or much shorter (for F^{7+} and Si^{12+}).

We measured DR in the range of relative energies 0 eV - 28 eV, where no structures related to the ground state was expected. The following DR reactions could be expected in this energy region: (We expect the first two of these to be dominant since their radiative core stabilization process is dipole-allowed.)



To be able to extract absolute rate coefficients from the measurements, it is necessary to know which fraction of the incoming

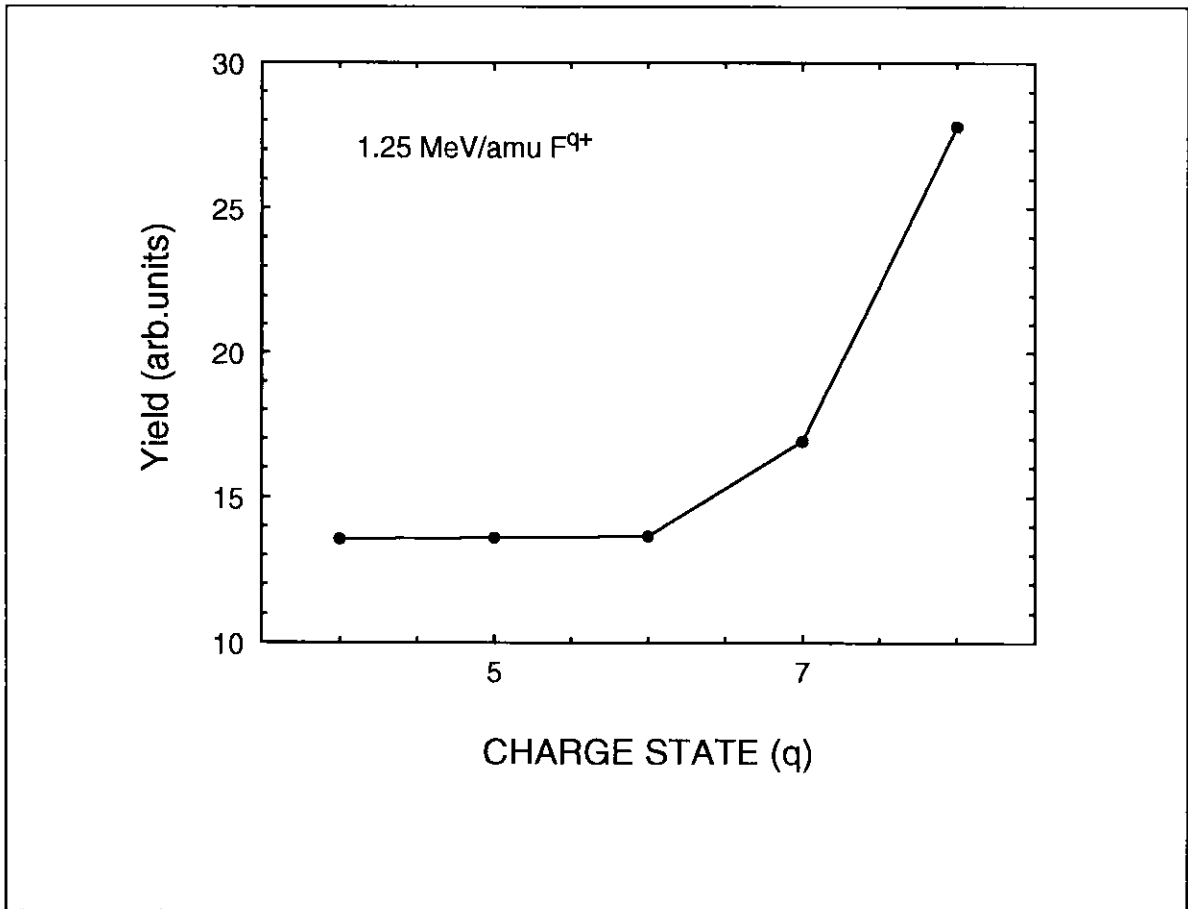


Figure 5.6 *Relative yield of Al K x rays for beams of flourine ions in different charge states q as a function of q .*

ions is in the different states. In order to enlighten this question, we performed a series of x ray experiments. The ion beam from the tandem accelerator was passed through a carbon foil coated with a thin layer of aluminum. The emitted Al K x rays were detected at a right angle using a Si(Li) x ray detector. The idea was to take advantage of the fact that the yield of K x rays is dramatically increased when ions with only one electron in the K shell are used. The result of a series of measurements with fluorine ions in different charge states is shown in fig.5.6. We note that the yield is constant for F ions with 3, 4, and 5 electrons, corresponding to no K-shell holes. If we now assume that the increase in the yield is solely due to the presence of K-holes, the

fraction of He-like ions in the 1s2s configuration can be determined by

$$\text{metastable fraction} = \frac{Y_{(\text{He-like})} - Y_{(\text{Li-like})}}{Y_{(\text{H-like})} - Y_{(\text{Li-like})}}. \quad (5.4)$$

Note that this gives the fraction at the Al target, and that no information is achieved as to how large a fraction of the ions in the 1s2s configuration is in the ^1S or ^3S state, respectively.

If the lifetimes of the 1s2s ^1S states (Drake 1969) as well as the ion flight times to the Al target and to the electron cooler, respectively, are taken into account, the assumption of statistical population in the production mechanism (three times as many ions in the 1s2s ^3S state as in the 1s2s ^1S state), leads to the following metastable fractions in the electron cooler.

Table 5.1

ion term	C ⁴⁺	N ⁵⁺	O ⁶⁺	F ⁷⁺	Si ¹²⁺
1s2s ^1S	3 % (foil)	2 %	1 %	0.2 %	0.004 %
1s2s ^3S	16 % (foil) 7 % (gas)	15 %	20 %	23 %	12 %

C⁴⁺ and O⁶⁺ were included in these measurements because DR for these ions had been studied earlier without knowledge of the metastable fractions (Andersen 1990, Badnell 1990).

Figure 5.7 shows the result of our DR measurement for N⁵⁺ together with an LS-coupling calculation performed by Badnell and Pindzola [III]. A ^3S population of 15% as determined above was used. The ^1S population had to be adjusted to 0.8% for the theory to fit the

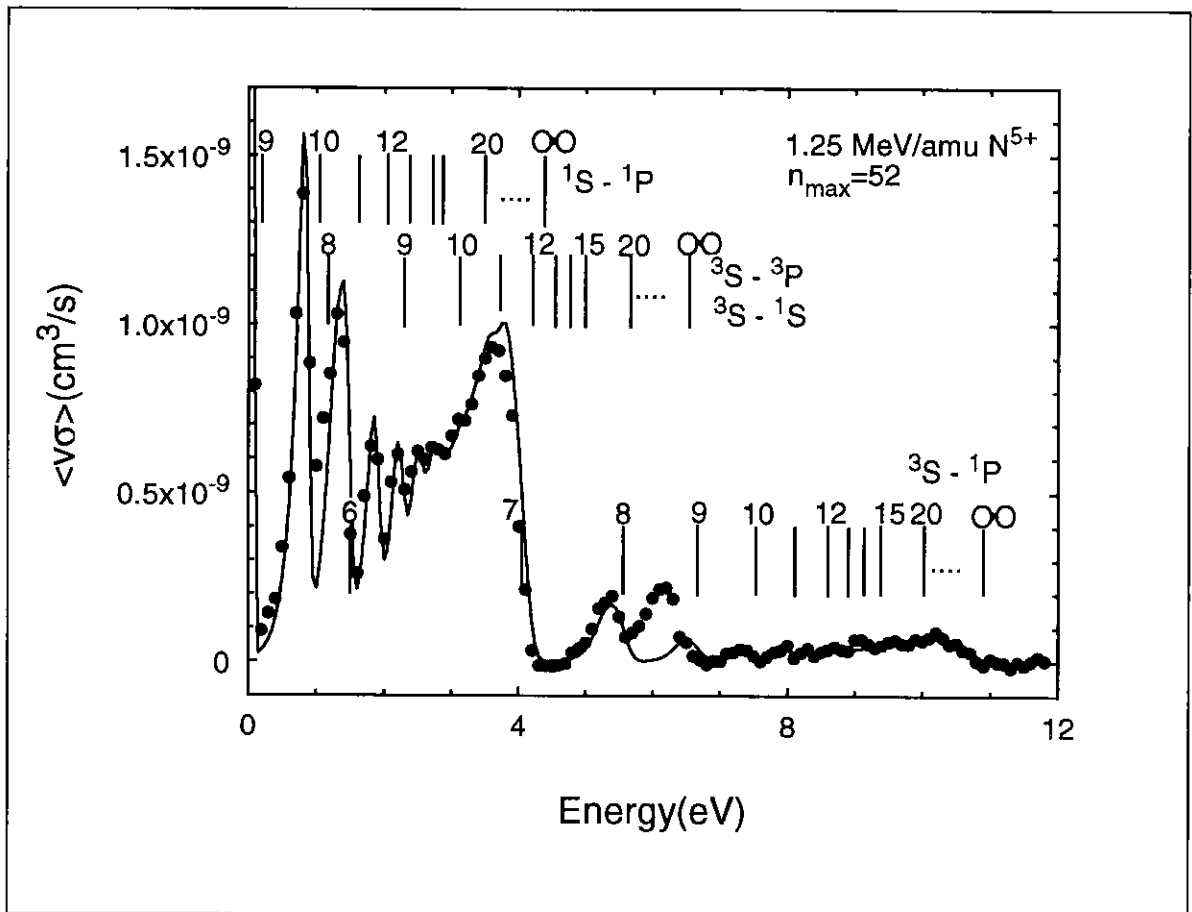


Figure 5.7 Measured and calculated rate coefficient of DR for N^{5+} ions. Metastable fractions of 0.8 % ($1s2s\ ^1S$) and 15 % ($1s2s\ ^3S$) were assumed in the calculations.

experiments on an absolute scale. If we assume that these are the right metastable fractions, agreement between theory and experiment is found except for an extra peak at about 6 eV. Except for this peak, what we see are two Rydberg series, one associated with the $1s2s\ ^1S \rightarrow 1s2p\ ^1P$ excitation, the other associated with the $1s2s\ ^3S \rightarrow 1s2p\ ^1P$ excitation. We notice that the contribution from the last of these two series is decreasing dramatically when states above the 3P and 1S series are considered. This is due to the fact that autoionization into these two open channels can now take place.

Concerning the extra peak at about 6 eV, we notice that also for

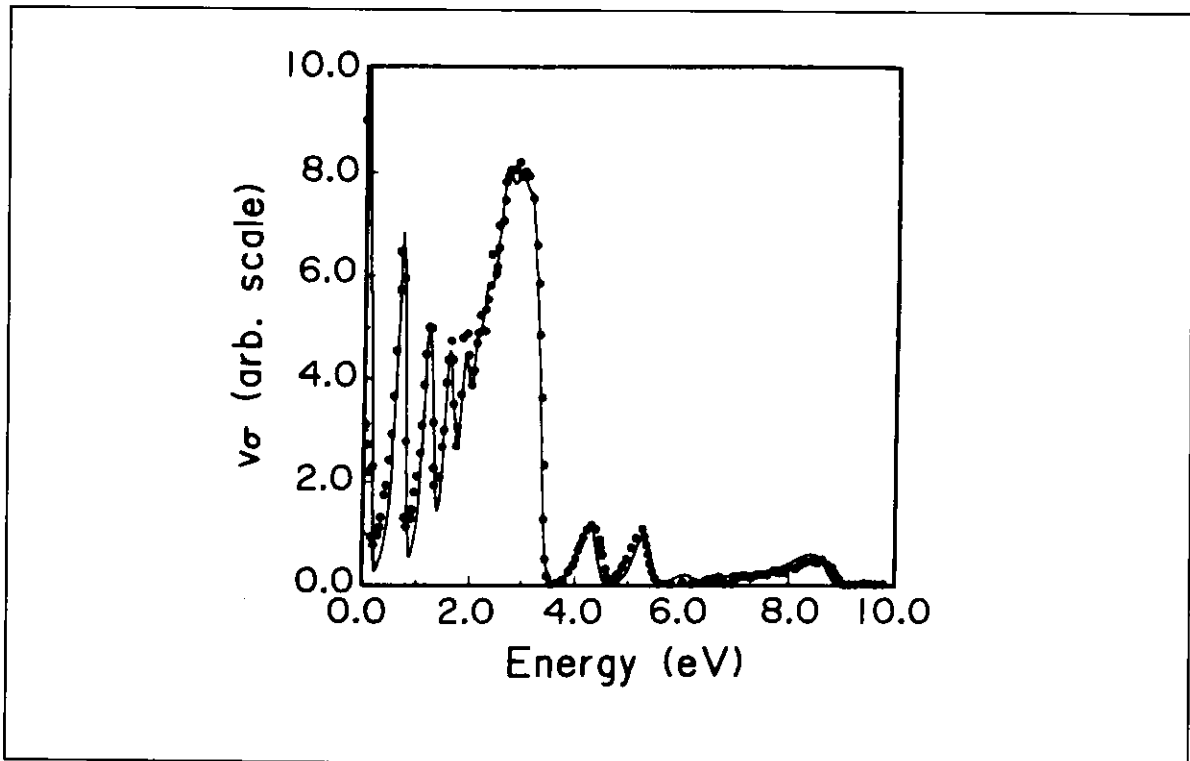
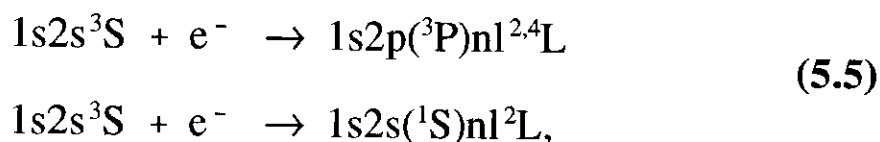


Figure 5.8 Illustration from (Badnell 1990) showing the apparently perfect agreement between theory and experiment for C^{4+} ions.

O^{6+} (Andersen 1989, Andersen 1990) and F^{7+} [III], an unexplained feature is seen just below the almost coincident 3P and 1S thresholds. It was therefore almost disturbing that for C^{4+} , absolutely perfect agreement was found between theory and experiment (see fig.5.8 and Badnell 1990). The key to this 'problem' turned out to be the $1s2p(^1P)8l$ configurations which were assumed to be responsible for the peak at about 5 eV in fig.5.8. All these configurations are found to be very close in energy to the $1s2s\ ^1S$ threshold (for $l=1$ or 2 ; too close for the theorists to determine which terms are above the $1s2s\ ^1S$ threshold). The terms higher in energy than the $1s2s\ ^1S$ threshold have a very high autoionization rate to the $1s2s\ ^1S$ continuum, and the DR cross section will be strongly reduced. In the original calculations (Badnell 1990), all the terms of the $1s2p(^1P)8p$ and $1s2p(^1P)8d$ configurations were found to be bound with respect to $1s2s\ ^1S$, and since

this gave results which agreed with experiment, it was of course believed to be correct. Later it turned out, however, that for theory to be able to account for the observed cross sections for DR for *ground state* C^{4+} (Kilgus 1991), it had to be assumed that all these terms were in fact *above* the $1s2s\ ^1S$ limit and could therefore autoionize into this continuum. This means that also for C^{4+} , there is a peak in the experimental data close to the 1S and 3P thresholds, not properly accounted for in the calculations.

In the following, possible explanations of this extra structure will be discussed. Since the energy position of a DR signal is determined by the initial capture process, and since the structure we want to account for is found just below the 1S and 3P thresholds, the responsible capture process(es) must be found among the following



where the principal quantum number of the captured electron must be larger than 20 for the energy-position to fit in the observed spectra. The problem with these capture processes is that the doubly excited intermediate states formed cannot decay directly to the $1s^2(^1S)nl$ configuration via an allowed electric-dipole transition. This means that we have to look for some other stabilization mechanism.

One such stabilization mechanism was proposed by Taulbjerg and Macek (Taulbjerg 1989) just after the first high-resolution DR measurement of O^{6+} (Andersen 1989). Their idea was that the intermediate states as described here were not pure states, but they

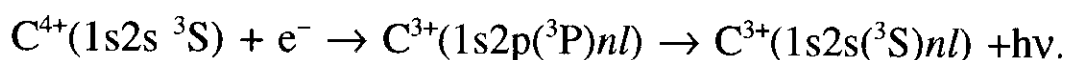
were 'contaminated' with close-lying levels of $1s2p(^1P)n'l'$ via configuration interaction. The states formed can formally be described as follows:

$$\begin{aligned} & [1s2p(^3P)nl + \varepsilon \cdot 1s2p(^1P)n'l']^2L \\ & [1s2s(^1S)nl + \varepsilon \cdot 1s2p(^1P)n'l']^2L \end{aligned} \quad (5.6)$$

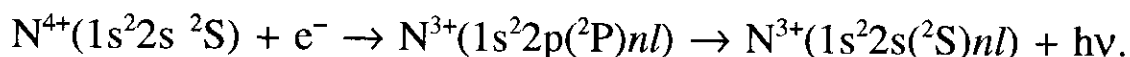
Here ε is meant to indicate that only a weak mixing is assumed. $L=l, l\pm 1$, $l'=l, l\pm 1$, and n' is 8 for C^{4+} , 9 for N^{5+} , and probably 10 for O^{6+} . Because of the presence of the $1s2p(^1P)$ core, these states can then stabilize radiatively to $1s^2(^1S)n'l'$. And this was then assumed to be the stabilization mechanism responsible for the observed DR signal.

For the first of the capture processes of eq.(5.5), another stabilization process could be the allowed electric-dipole transition to $1s2s(^3S)nl\ ^2L'$, $L'=L, L\pm 1$. This is not really a stabilization process since this state can still autoionize to the ground state $1s^2\ ^1S$ and a high-energy electron (≈ 300 eV for C^{4+}), but in particular the quartet terms may be sufficiently long-lived to survive until after the charge-state analysis and therefore be counted as recombined. Dielectronic capture, followed by transitions to metastable autoionizing states, has also been seen in other DR measurements. As an example of this, we mention the situation for Be-like ions [I], where it was found that about 50% of the ions that ended up in the metastable autoionizing $1s^2s2p(^3P)nl$ state were actually counted as recombined because they had not autoionized before the charge-state analyzer. The idea that this mechanism could also be responsible for the extra structure in the He-like ions is in fact mentioned in [I], but based on a qualitative comparison with the dominant series caused by the 3S metastables

($1s2s\ ^3S + e^- \rightarrow 1s2p(^1P)nl \rightarrow 1s^2(^1S)nl$), it was concluded that this mechanism could be neglected. Nevertheless, the following considerations will show that assuming a large survival probability of the metastable autoionizing states, the proposed mechanism does indeed give rise to a DR signal of the right order of magnitude. For C^{4+} , the maximum rate coefficient in the extra peak amounts to approximately $8 \cdot 10^{-10}$ cm³/s with the experimental velocity distribution. The proposed mechanism is the following:



We now assume that a reasonable measure of the rate coefficient for this process can be obtained by considering the situation, where an inactive 1s electron is added to the electronic core, and to compensate for the charge of this electron, a proton is added to the nucleus. This system is Li-like nitrogen which was already considered in the previous section



We see that apart from possible effects of spin, these two processes are very similar, and the maximum of the experimental rate coefficient found for N^{4+} was $6 \cdot 10^{-10}$ cm³/s, indicating that the proposed mechanism may give rise to a DR rate coefficient of the right strength.

This means that we have now two different explanations of the extra structure, and on the basis of the experimental results presented so far, we are not able to tell which one is correct. But there is an important difference between the two proposed mechanisms. In the

case of configuration interaction, the final state is a Rydberg state with $n \leq 10$ ($n=8$ for C^{4+}), whereas the proposed metastable autoionizing states will have a Rydberg electron keeping the same principal quantum number that it was captured into, and this must be $n \geq 20$. This means that if the experiment is done again, and this time with a stronger analyzer field, leading to field ionization for all ions with $n \geq 20$, the extra structure will disappear if the mechanism is radiative transition to a metastable autoionizing state, whereas in the case of the configuration-interaction mechanism, this structure will remain unchanged.

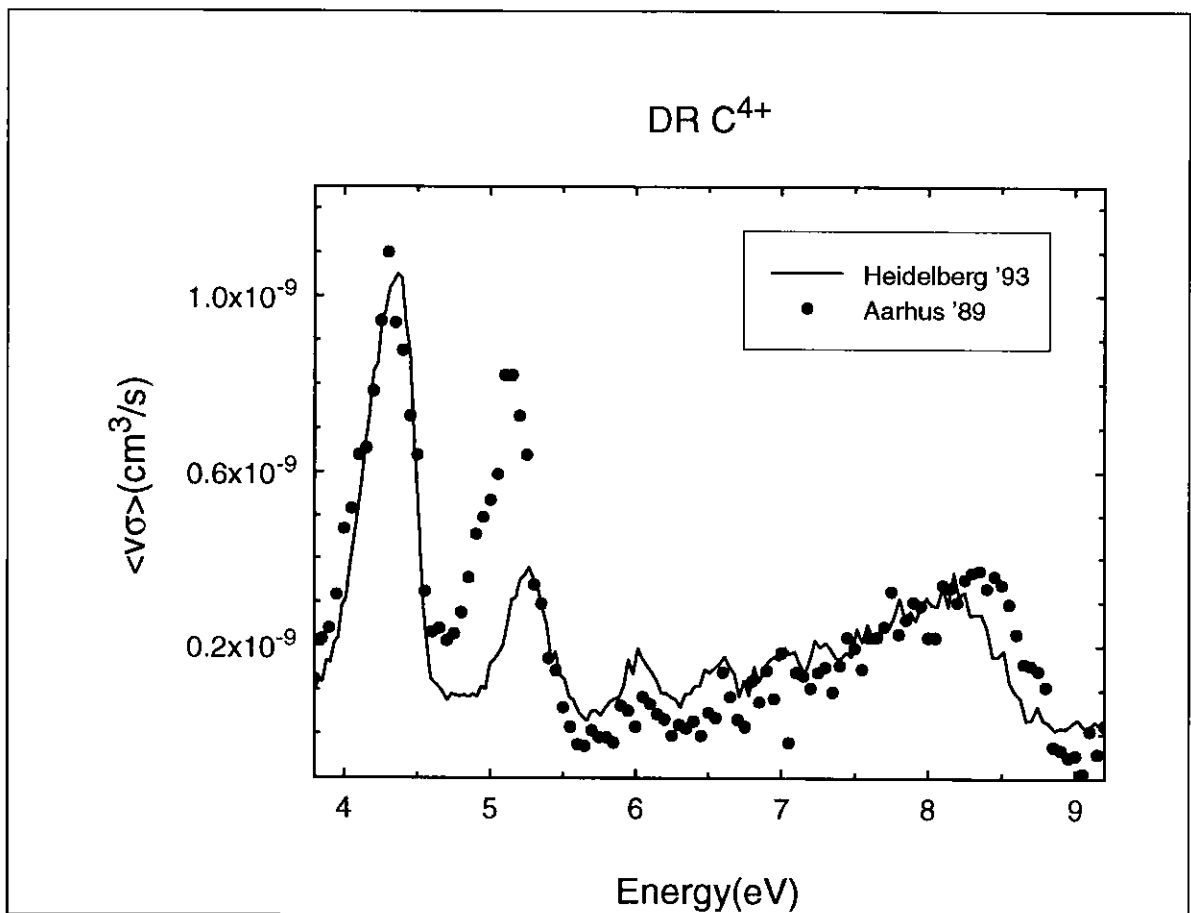


Figure 5.9 Comparison of the two results of DR measurements for He-like C^{4+} . The strong reduction of the peak at 5 eV is taken as evidence for the proposed mechanism (see text).

The storage-ring experiments described in the following section

represent just this new measurement of DR for He-like boron, carbon, and oxygen ions in the $1s2s\ ^3S$ state. In fact, in the case of C^{4+} , the limit for field ionization as given by eq.(3.2) amounts to $n_{\text{limit}}=20$. Figure 5.9 shows the measured DR rate coefficient for C^{4+} in the vicinity of the structure just discussed. We see that this structure is strongly reduced in the storage-ring experiment as compared to the earlier single-pass result. Following the discussion given above, we therefore conclude that the extra structure observed in the single-pass experiment is caused by initial capture to $1s2p(^3P)nl$ states, followed by a radiative transition to metastable autoionizing states of the form $1s2s(^3S)nl$ rather than by configuration interaction.

5.4 DR for metastable He-like ions (the TSR experiment)

For the TSR experiments, the He-like ions were created in the stripping target of the 12 MV tandem accelerator used as injection accelerator for this facility. Just as in the single-pass experiment, this leads to population of the metastable $1s2s\ ^{1,3}S$ states, but since the metastable singlet states of the ions involved (B^{3+} , C^{4+} , and N^{5+}) have lifetimes only of the order of a few μs , we get a pure spectrum of contributions only from the metastable triplet state by waiting about one ms after injection into the storage ring before we start taking data. The beam energies applied were 44 MeV for B^{3+} , 55 MeV for C^{4+} , and 60 MeV for N^{5+} . And the storage lifetimes limited by collisions with residual gas molecules (typical vacuum $5\cdot 10^{-11}$ mBar) were in all cases of the order of one to three minutes.

When usual experiments with ions in the ground state are

performed at the TSR, one applies the so-called multi-turn injection which makes the intensities of stored ion beams larger than the intensity in the injection accelerator beam by a factor of up to 40 (Bisoffi 1990). This leads to a very large horizontal ion-beam width, which is normally not a problem since a very narrow beam can be obtained by applying electron cooling for a few seconds before starting the actual measurement. However, in our case, where we want to measure the DR signal for ions in metastable states with lifetimes in the ms range this method is not applicable. On the other, hand if we tried to do the experiment with a normal multi-turn-injected ion beam, we would find ourselves in the rather unpleasant situation of having an ion beam which had a larger diameter than the aperture of our detector (2.5 cm in the horizontal direction). To circumvent this problem, we take advantage of the fact that in a normal multi-turn injection, those ions first injected will have the smallest amplitude in their oscillations around the ideal closed orbit of the storage ring (betatron oscillations). It is therefore possible to reduce the size of the ion beam in the horizontal direction by interrupting the injection at a properly chosen time. By doing so, the horizontal ion-beam width could be reduced from about 4 cm to about 1.2 cm, as observed on the TSR beam-profile monitor, making it simple to ensure that all particles, which had captured an electron on the electron-cooler straight section of the storage-ring, would be detected on the moveable multi-channel-plate detector.

The beam-profile monitor works in the following way: The passage of multiply charged ions through the residual gas leads to ionization of residual-gas molecules, which can then be electrostatically accelerated towards a position sensitive channel-plate

detector, thereby yielding the projection of the beam profile onto one of the transverse directions (Hochadel 1990). At the same time, the total count rate on the beam-profile monitor will be proportional to the ion current and may therefore be used as a relative measure of this.

With the injection scheme described above, typical currents of the stored ion-beams were a few μA 's, which is slightly too low for a reliable ion-current measurement to be performed with the DC current transformer installed for this purpose. We therefore made a calibration of the counts from the beam-profile monitor versus the DC current transformer by going to high currents, applying the normal multi-turn injection. We could then use the beam-profile monitor for measuring the currents in the experiments within systematic errors of approximately 30%.

For C^{4+} and N^{5+} with metastable lifetimes of 20 ms and 4 ms, respectively, ions were injected at the maximum injection rate of 4.8 Hz to optimize the time-averaged number of metastable ions in the storage ring. For B^{3+} with a metastable lifetime of about 150 ms, a new injection was made every 800 ms.

To match the velocities of the ion beams just described, the electron energies were typically about 2.5 keV. Typical electron currents were around 250 mA, which with a beam diameter of 5 cm corresponds to an electron density of $2\text{-}3 \cdot 10^7 \text{ cm}^{-3}$. This is similar to the electron densities in the Aarhus single-pass experiment (sec.3.2). The electron-beam position was optimized by making electron cooling of a stored ion beam. The relative positions of the ion and electron beams could be optimized by finding a minimum, for a given electron-beam acceleration voltage, of the ion-revolution frequency, as observed in the Schottky spectrum. This minimum corresponds to the situation

where the ions pass through the center of the electron beam where the space-charge potential given by eq.(3.23) is at maximum (numerically), and therefore the electron velocity is at minimum. The angular alignment was made by minimizing the ion-beam width, as observed on the beam-profile monitor, since better alignment means lower average relative velocity and hence more effective transverse cooling, leading to smaller beam size. After this alignment procedure, the acceleration voltage corresponding to the cooling energy could be determined, and it was checked that taking into account the space-charge potential as given by eq.(3.23) gave the proper electron velocity. This indicated that the space-charge correction was done correctly, and the ion beam was in fact passing through the center of the electron beam. With this information, it is possible to deduce the relative energies from the recorded values of the acceleration voltages and electron currents.

The DR measurement was performed as follows: The acceleration voltage was set to a given value by the electron-cooler control computer. After each injection, the number of particles detected by the channel-plate detector were counted in two time windows. One starting about one ms after the injection and lasting for a time corresponding to about one lifetime of the 3S state of the He-like ion to measure the DR signal, and another time window starting after several 3S lifetimes to measure the background contribution which was typically about 10% of the DR signal at a major resonance. This was repeated for about 20 injections, whereupon the number of counts in the two time gates, the actual gate times, the electron acceleration voltage, the electron current, and the ion current in terms of the total number of counts on the beam profile monitor were stored on a μ -

VAX computer, and the electron acceleration voltage was stepped to the next value for measuring.

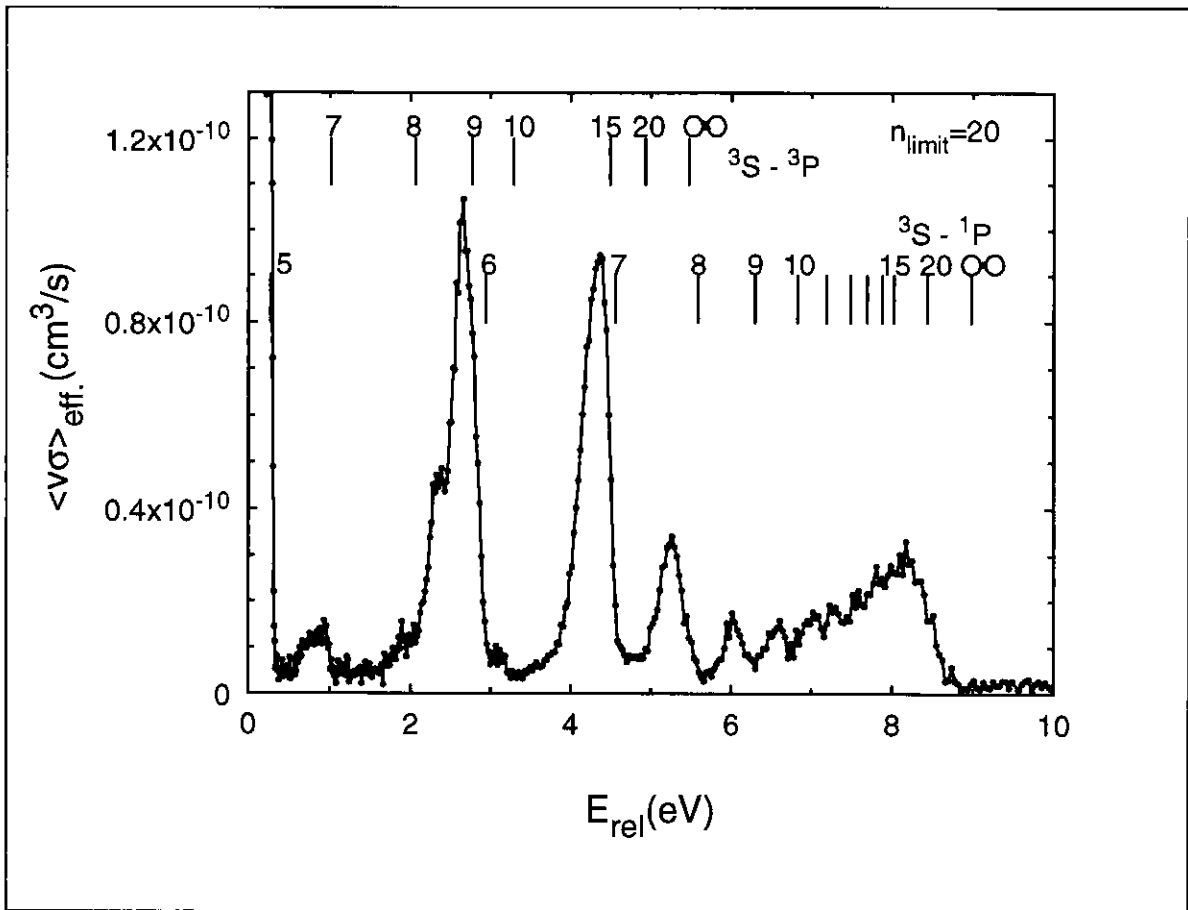


Figure 5.10 The measured effective rate coefficient for DR for C^{4+} ions in the metastable $1s2s\ ^3S$ state.

Figure 5.10 shows the result of the DR measurement for C^{4+} in terms of the *effective* rate coefficient obtained by pretending in the analysis that the unknown average fraction of metastables during the signal time window is 100%. By comparing this to the theoretical rate coefficient (Badnell 1990), which was confirmed in the single-pass experiments, the average metastable fraction can be deduced, and from knowledge of the metastable lifetime and the gate-open and -close times, the initial metastable fraction is found. The result for C^{4+} was 18(6)%, where the main source of error comes from the ion-current

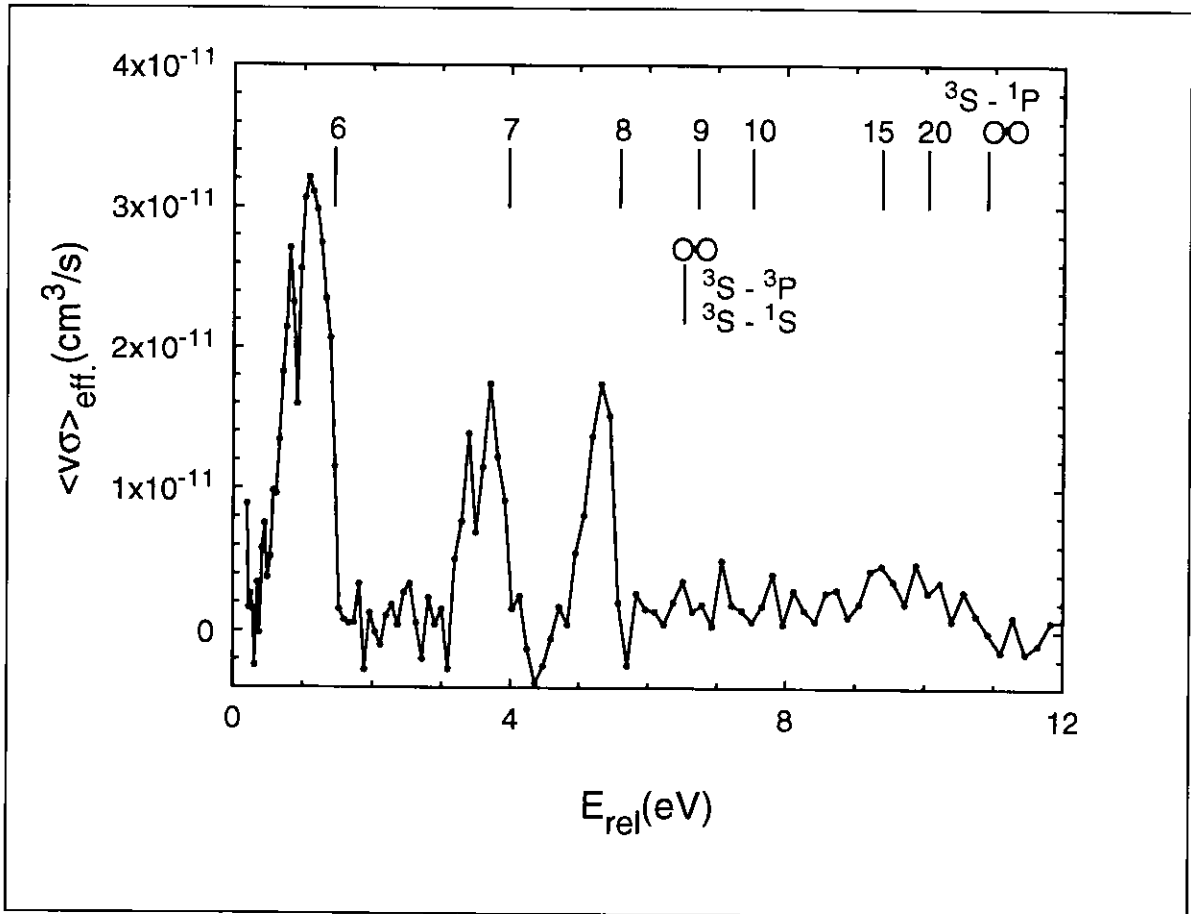


Figure 5.11 The measured effective rate coefficient for DR for N^{5+} ions in the metastable $1s2s\ ^3S$ state.

measurement.

With no contribution from the 1S metastables, the observed DR spectrum is dominated by the series of resonances related to the excitation from $1s2s\ ^3S$ to $1s2p\ ^1P$. Single resonances can be resolved up to the principal quantum number of the captured electron $n'=12$. Details of the $n'=5$ peak close to 0 eV could not be observed due to the substantial drag force at low energy. For the $n'=6$ peak, we observe a splitting caused by the different l -quantum numbers of the captured electrons. The DR signal for $n' \geq 8$ is reduced because of the opening of new autoionization channels, as discussed in the previous section. The high- n' contribution is only slightly reduced due to the stronger

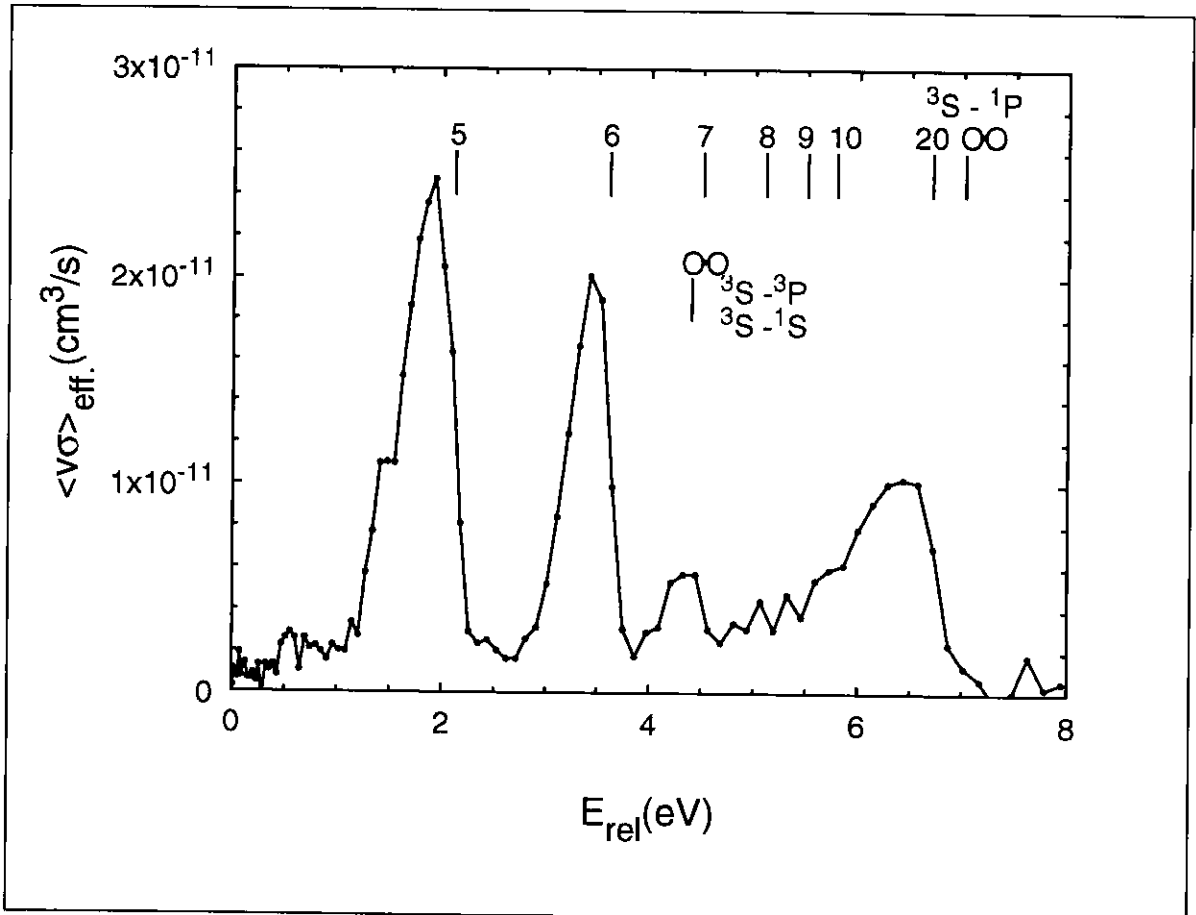


Figure 5.12 The measured absolute rate coefficient for DR for B^{3+} ions in the metastable $1s2s\ ^3S$ state.

field-ionization effects as compared to the single-pass experiment. This is because the stabilization mechanism is a $\Delta n=1$ process, where the high- n' contribution is known to be small (see sec.5.1).

This is in strong contrast to the high- n' contribution related to the 3S - 3P excitation which, as discussed in sec.5.3, becomes strongly reduced going to the lower n_{limit} of the storage-ring experiment, yielding yet an indication that the stabilization for this process is in fact a $\Delta n=0$ transition (i.e. a transition to $1s2s({}^3S)nl$). The only structure related to this excitation, which can be seen clearly in fig.5.10, is the peak just below 1 eV which we ascribe to the $n'=7$ -resonance of this excitation. The other resonances are hidden by the

much stronger DR signal related to the $^3S-^1P$ excitation.

In figs.5.11 and 5.12, the equivalent results for B^{3+} and N^{5+} are shown. For N^{5+} , the metastable fraction could be determined by comparing with the theoretical spectrum. When using a stripper gas at the tandem terminal (as was done for C^{4+}), the metastable fraction was as low as 3.1(1.0)%, whereas replacement of the gas by a thin foil leads to an increase to 11(4)%. For B^{3+} , no detailed calculation was available for comparison, but by extrapolating the rate coefficients from the known values for He-like carbon, nitrogen, and oxygen, the metastable fraction was found to be of the order of 10%.

Let us end this section on the DR measurements of stored, metastable He-like ions by concluding that they appear to be well understood and have shed light on a five year old controversy regarding certain anomalies observed in the Aarhus single-pass experiment.

5.5 DR for Be-, B-, and C-like ions

This short section on DR for Be-, B-, and C-like ions is only added for completeness. For a detailed discussion of these, reference is made to the original articles [I,V].

As was the case for the He-like ions, the presence of ions in metastable states in the single-pass experiment was found to strongly influence the observed DR spectra. But unlike the situation for He-like ions, the excitation to the metastable states is an intra-shell ($\Delta n=0$) excitation which requires only a small amount of energy. This means that at low relative energies, both DR for metastable and ground states

will be observed.

As an example I show here the observed recombination spectrum for C-like flourine ions (fig.5.13). DR related to ions initially in all three terms (3P , 1D , and 1S) of the ground-state configuration $1s^22s^22p^2$ is observed. The observed spectrum relates to the following three single-electron excitations: $2s-2p$, $2p-3s$, and $2p-3d$.

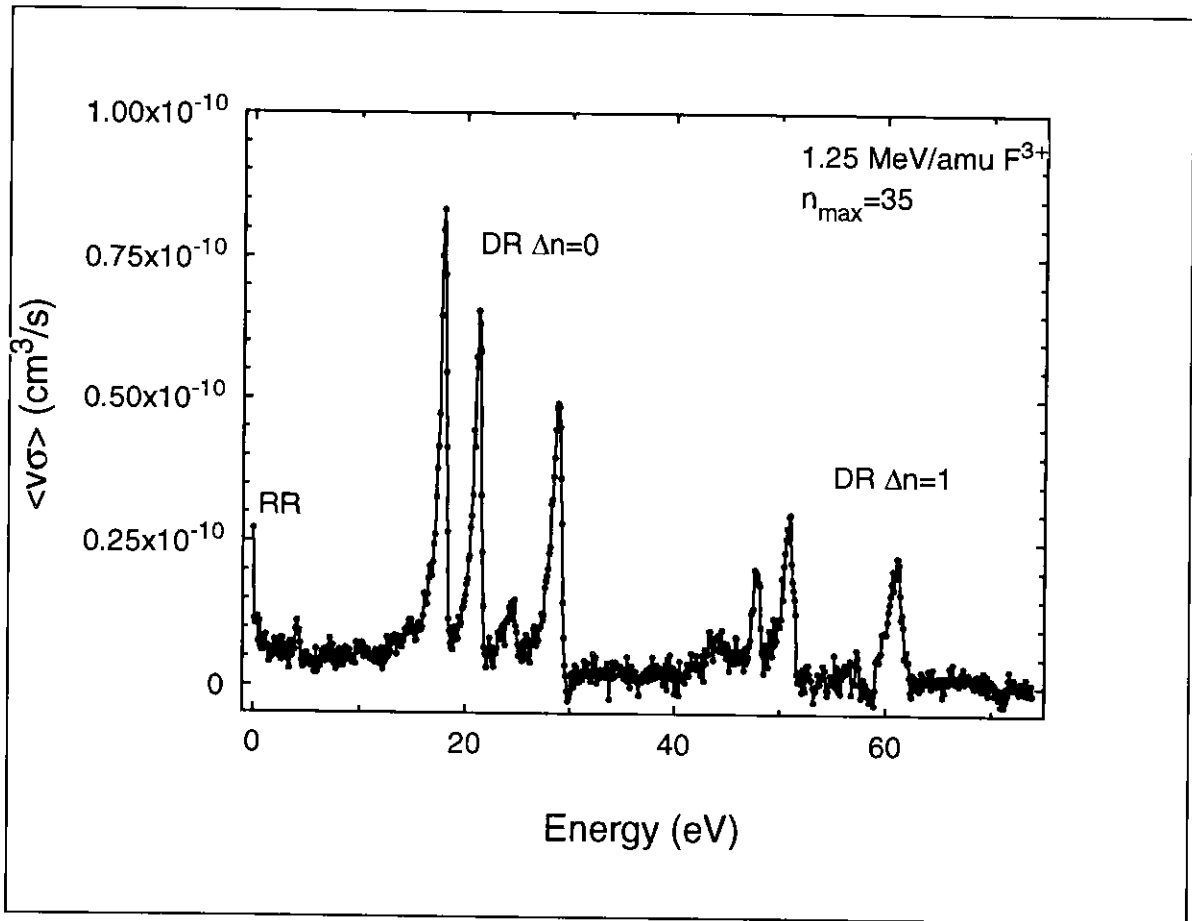


Figure 5.13 Complete recombination spectrum of F^{3+} in the energy range of 0 eV to 74 eV. Contributions from RR, DR($\Delta n=0$), and DR($\Delta n=1$) can be observed.

- R Ali, C P Bhalla, C L Cocke, M Schulz and M Stockli (1991) Phys.Rev.A 44 223*
- L H Andersen, P Hvelplund, H Knudsen, and P Kvistgaard (1989) Phys.Rev.Lett. 62 2656*
- L H Andersen, J Bolko and P Kvistgaard (1990) Phys.Rev. A 41 1293*
- N R Badnell, M S Pindzola, and D C Griffin (1990) Phys.Rev.A 41 2422*
- P Beiersdorfer, M H Chen, R E Marrs, M B Schneider and R S Walling (1991) Phys.Rev.A 44 396*
- G Bisoffi, M Grieser, E Jaeschke, D Krämer, and A Noda (1990) NIM A287 320*
- P F Dittner, S Datz, P D Miller, C D Moak, P H Stelson, C Bottcher, W B Dress, G D Alton, N Neskovic and C M Fou (1983) Phys. Rev. Lett. 51 31*
- G W F Drake, G A Victor and A Dalgarno (1969) Phys.Rev. 180 25*
- G W F Drake (1971) Phys.Rev.A 3 908*
- D C Griffin (1989) Physica Scripta T28 17*
- Y Hahn (1994) Submitted to Phys.Rev.A*
- B Hochadel (1990) Thesis entitled: "Ein Strahlprofilmonitor nach der methode der Restgasionisation für den Heidelberger Testspeicherring TSR, Max-Planck Institut für Kernphysik, Heidelberg."*
- G Kilgus, D Habs, D Schwalm, A Wolf, R Schuch, N R Badnell (1993) Phys.Rev.A 47 4859*
- J B A Mitchell, C T Ng, J L Forand, D P Levac, R E Mitchell, A Sen, D B Miko, and J Wm McGowan (1983) Phys.Rev:lett. 50 335*
- A Müller, D S Belic, B D DePaola, N Djuric, G H Dunn, D W Mueller and C Timmer (1987) Phys.Rev.A 36 599*
- W Spies, A Müller, J Linkemann, A Frank, M Wagner, C Kozhuharov, B Franzke, K Beckert, F Bosch, H Eickhoff, M Jung, O Klepper, W König, P H Mokler, R Moshhammer, F Nolden, U Schaaf, P Spaedtke, M Steck, P Zimmerer, N Grun, W Scheid, M S Pindzola, N R Badnell (1992) Phys.Rev.Lett. 69 2768*
- K Taulbjerg and J Macek (1989) Phys.Rev.Lett. 62 2766*
- A Wolf, J Berger, M Bock, D Habs, B Hochadel, G Kilgus, G Neureither, U Schramm, D Schwalm, and E Szmola (1991) Z.Phys.D 21 69*

6. Lifetime measurements based on DR

For the TSR DR measurements described in sec.5.4, we took advantage of the fact that the ions in the metastable states decayed to the ground state and therefore no longer contributed to the DR signal in the energy range considered. This allowed us to isolate the background signal by waiting for (practically) all the ions in the metastable state to decay to the ground state. In this chapter, experiments are discussed in which we determine the lifetimes of the metastable states by recording the time dependence of the recombination signal.

In sec.6.1, an introduction to this subject is given, and earlier experimental results are quoted. Section 6.2 describes the experimental procedure, and in sec.6.3, the data analysis is described. Finally, discussion and comparison with theory are presented in sec.6.4. The results for carbon and nitrogen were presented in [VI], whereas the boron result has not been published before.

6.1 Lifetime of the 3S metastable state of He-like ions

We consider spontaneous radiative transitions in the He-like atomic systems from the lowest excited state $1s2s\ ^3S_1$ to the ground state $1s^2\ ^1S_0$. Due to conservation of the total angular momentum of the entire system (including the radiation field), a triangle inequality of the final and initial total angular momentum J of the atomic system and the multipole order of the emitted radiation must be fulfilled (Marrus 1978). As J goes from one to zero, this means that the emitted

radiation is of order one, i.e. we have a dipole transition. As the parity does not change, an electric-dipole (E1) transition can be excluded, and we are left with a magnetic-dipole (M1) transition as the only possible one-photon mechanism. A spin-forbidden two-photon E1 transition cannot be ruled out and was in fact for almost 30 years believed to be dominating (Breit 1940). But after the identification of spectral lines associated with the M1 decay of He-like ions in the radiation emitted from the solar corona (Gabriel 1969, 1970), theoretical studies of the M1 decay were actively pursued (Beigman 1971, Drake 1971, Feinberg 1971, Johnson 1974). It was then found that the M1 decay was the dominating decay mode of the 2^3S state for all He-like ions, and in particular for the ions of boron, carbon, and nitrogen considered here, it was found that the ratio of the rate of the two-photon E1 transition to that of the M1 transition is about $2 \cdot 10^{-4}$ (Drake 1969, 1971).

The 2^3S decay rates of He-like ions with high nuclear charge ($Z \geq 16$) in the range $> 10^6 \text{ s}^{-1}$ were measured in a number of experiments using the beam-foil technique (Marrus 1978, Hubricht 1987, Marrus 1989). This yielded results with experimental errors of $\geq 3\%$ which did not distinguish between the different theoretical approaches to the problem. Much less data are available for He-like systems with lower Z , where the M1 decay rate, scaling roughly as $\propto Z^{10}$, becomes small ($\approx 10^{-4} \text{ s}^{-1}$ for He). On the other hand, especially for the low- Z systems, the Coulomb interaction between the two electrons is expected to have large effect and to add a further complication to the calculation of the M1-transition matrix element, whereas in the high- Z systems mainly studied experimentally until now, two-electron effects lead to small corrections only.

Measurements of the 2^3S decay rate in low- Z He-like systems

have so far been performed for He atoms (Woodworth 1975) and Li^+ ions (Knight 1980). Due to the very low decay rates for these two ions, it was not possible to use the time dependence of a signal related to the 2^3S states. Instead, the decay rate was deduced from observation of the emitted photons from the M1 decay, in combination with a probe measurement to determine the number of ions in the metastable state. Here, the correction to the transition matrix element due to the electron-electron interaction (Drake 1971) is of the order $\approx 30\%$, but experiments have confirmed the expected size of this correction with low precision only, limited by errors of 15-20%. Recently, an experiment on Ne^{8+} ions was performed with an electron-beam ion trap (Wargelin 1993). Here the two-electron correction is $\approx 5\%$, and with an experimental error of 1.7%, this experiment has somewhat improved the situation for low-Z He-like ions.

The experiments treated in this chapter for boron, carbon, and nitrogen have relative errors of 2.8‰, 2.3‰, and 1.2‰, respectively, and for the first time, distinction between the theories of Drake (Drake 1971) and of Johnson and Lin (Johnson 1974) can be made.

6.2 The experiment

The lifetime measurements were performed at the TSR during the same beam times as the DR measurements described in sec.5.4. When the DR spectrum was recorded for the currently studied He-like ion, the electron acceleration voltage was fixed at a value corresponding to one of the resonances, and we changed data taking system to a multichannel scaler which, recorded as a function of time after the

injection, the number of particles hitting the channel-plate also used for the DR-measurement. The time scale was shown to be reproducible within relative deviations of $<10^{-3}$ for carbon and nitrogen. Prior to the boron experiment, this was improved to $<2 \cdot 10^{-5}$. Measurements were performed at different resonances to exclude a dependence of the measured decay rate on the relative energy, which might be suspected due to the small drag force exerted on the ions by the electron beam (see sec.3.2).

The decay curve measured on the C^{4+} , $n'=6$ peak after adding up

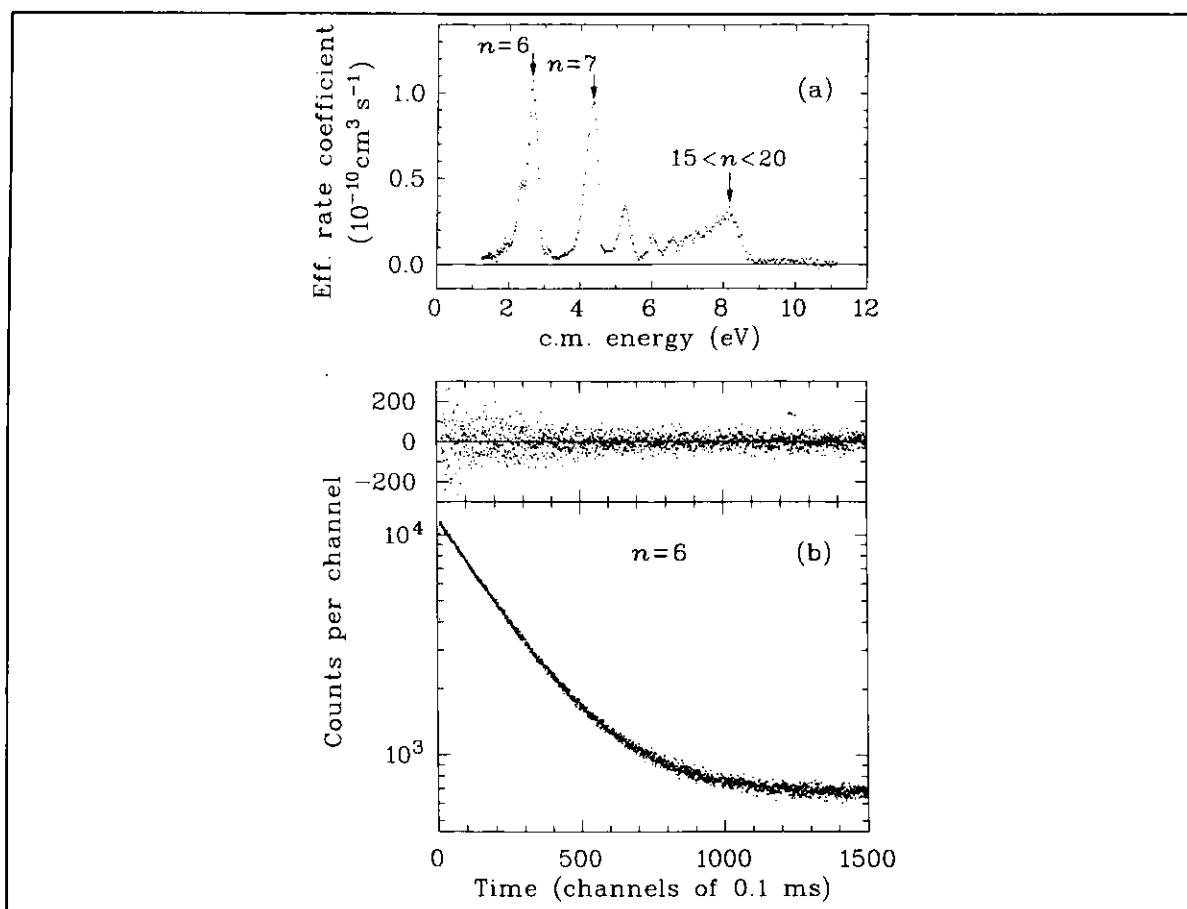


Figure 6.1 (a): The C^{4+} DR spectrum, with indications of the resonances where decay curves were recorded. (b): Decay curve recorded at the $n'=6$ resonance and deviations from the fit to eq.(6.4).

approximately 70 000 injections is shown in Fig.6.1. Because of the long beam lifetime of ≈ 2 min and the small influence of any collisional processes, the signal features a very clean exponential decrease due to the radiative decay of the 2^3S state.

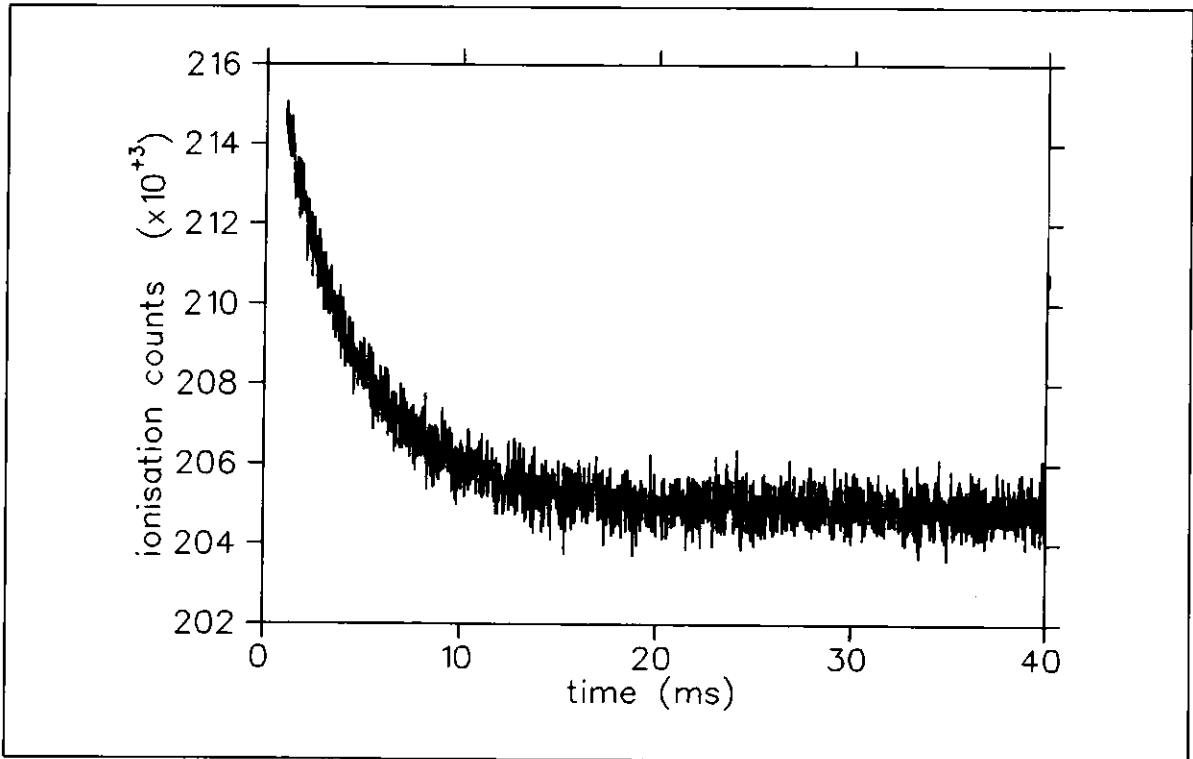


Figure 6.2 Yield of N^{6+} ions formed in residual-gas collisions in the electron-cooler straight section as a function of time after injection of a N^{5+} beam.

In the case of C^{4+} and N^{5+} , an additional detector was counting the ions which had lost an electron due to ionizing collisions with residual-gas molecules, and this information was recorded by the multi-channel scaler as well. It was demonstrated that due to the large difference in the ionization cross sections of ions in the metastable and ground states, lifetime measurements of poorer but comparable quality could have been performed by considering this signal rather than the DR signal. Figure 6.2 shows the yield of N^{6+} ions as a function of time after injection of a N^{5+} beam. Note the poorer 'signal-to-background'

ratio as compared to fig.6.1.

6.3 Analysis of data from the decay rate measurement

To extract from the data a precise value of the total radiative decay rate observed in laboratory rest frame, we must consider the following set of rate equations:

$$\begin{aligned} \frac{dN^m}{dt} &= -(A_r + A_l^m + A_q + A_{DR})N^m + A_e N^g, \\ \frac{dN^g}{dt} &= (A_r + A_q)N^m - (A_l^g + A_e)N^g, \end{aligned} \tag{6.1}$$

where N^m and N^g denote the population of the metastable $1s2s\ ^3S$ state (m) and the $1s^2\ ^1S$ ground state (g), respectively, and A_r is the radiative decay rate of the 3S state. All other rates in these equations are much smaller than A_r and describe the loss of ions from the storage ring for the two states ($A_l^{g,m}$), the collisional excitation from g to m (A_e), the collisional quenching from m to g (A_q), and the dielectronic recombination of the metastable ions (A_{DR}). The beam loss-rates $A_l^{g,m}$ are dominated by ionization of the circulating ions in collisions with residual-gas molecules. Different loss rates are assumed for the two state, since the ionization cross sections are larger for ions in the metastable state than for ground-state ions.

To solve these equations, we shall write them in the simpler form:

$$\begin{aligned} \mathbf{u}' &= \mathbf{a}\mathbf{u} + \mathbf{b}\mathbf{v}, \\ \mathbf{v}' &= \mathbf{c}\mathbf{v} + \mathbf{d}\mathbf{u}, \end{aligned} \quad (6.2)$$

where differentiation with respect to time is denoted by a prime and $\mathbf{u}=\mathbf{N}^m$, $\mathbf{v}=\mathbf{N}^g$, $\mathbf{a}=-(\mathbf{A}_r+\mathbf{A}_1^m+\mathbf{A}_{DR}+\mathbf{A}_q)$, $\mathbf{b}=\mathbf{A}_e$, $\mathbf{c}=-(\mathbf{A}_1^g+\mathbf{A}_e)$, and $\mathbf{d}=\mathbf{A}_r+\mathbf{A}_q$.

The solution to these equations is that both \mathbf{u} and \mathbf{v} will be linear combinations of the two exponentials $\exp(\mathbf{X}^+t)$ and $\exp(\mathbf{X}^-t)$ where

$$\mathbf{X}^\pm = \frac{1}{2} \left(\mathbf{a} + \mathbf{c} \pm (\mathbf{a} - \mathbf{c}) \sqrt{1 + 4\mathbf{b}\mathbf{d}(\mathbf{a} - \mathbf{c})^{-2}} \right). \quad (6.3)$$

The observed count rate, consisting of the dielectronic-recombination signal and a background contribution primarily caused by electron capture in residual-gas collisions, will again be a linear combination of \mathbf{u} and \mathbf{v} and can hence be represented as a function of time by the following two-component exponential:

$$\mathbf{F}(t) = \mathbf{C}_1 \exp(\mathbf{X}^+ t) + \mathbf{C}_2 \exp(\mathbf{X}^- t), \quad (6.4)$$

where \mathbf{C}_1 and \mathbf{C}_2 are arbitrary constants.

So far, we have made no approximations. To proceed, we now take advantage of the known orders of magnitude of the single terms. $\mathbf{A}_r \approx 7 \text{ s}^{-1}$, 50 s^{-1} , and 250 s^{-1} for B^{3+} , C^{4+} , and N^{5+} , respectively. For all the three ions considered here $\mathbf{A}_1^{g,m}$ are of the order 10^{-2} s^{-1} , $\mathbf{A}_{DR} \approx 10^{-3} \text{ s}^{-1}$, and $\mathbf{A}_{e,q} \leq 10^{-4} \text{ s}^{-1}$.

In the limit $\mathbf{A}_e = \mathbf{A}_q = 0$, we find $\mathbf{X}^+ = \mathbf{a} = -(\mathbf{A}_r + \mathbf{A}_1^m + \mathbf{A}_{DR})$ and $\mathbf{X}^- = \mathbf{c} = -\mathbf{A}_1^g$. This relation between \mathbf{X}^+ and \mathbf{X}^- means that we can

determine X^- by considering $F(t)$ after a few seconds when the first term has vanished. We therefore made a few long-time scans to determine X^- which was then kept fixed when the data from short scans of 5-10 radiative lifetimes were analyzed. A χ^2 method was applied to find X^+ with statistical errors from the data set.

Expanding eq.6.3 to first order in $A_{e,q}/A_r$ we find $X^+ \approx a + bd(a-c)^{-1} \approx -(A_r + A_1^m + A_{DR} + A_q + A_e(1 + A_1^m/A_r + A_{DR}/A_r + A_1^g/A_r)^{-1})$. We neglect terms of relative order $A_e A_1^{g,m}/(A_r)^2$ and find $X^+ \approx -(A_r + A_1^m + A_{DR} + A_q + A_e)$. Hence, to find A_r , we have to make estimates of A_1^m , A_{DR} , A_q , and A_e and subtract these from $|X^+|$.

For nitrogen, the result of the fit was $|X^-| = 6.0(2) \cdot 10^{-3} \text{ s}^{-1}$, and $|X^+| = 254.9(3.1) \text{ s}^{-1}$ (the errors stated here and throughout this section are one standard deviation). The leading correction A_1^m is of the same order as $A_1^g \approx |X^-|$ and thus more than two orders of magnitude smaller than the statistical uncertainty of X^+ . We therefore neglect the corrections and find $A_r = |X^+| = 254.9(3.1) \text{ s}^{-1}$. Correcting for the relativistic time dilation of the 60 MeV $^{14}\text{N}^{5+}$ beam yields the result $A_{CM}^N = 256.1(3.1) \text{ s}^{-1}$.

For carbon, the result of the fit was $|X^-| = 7.8(7) \cdot 10^{-3} \text{ s}^{-1}$, and $|X^+| = 48.350(95) \text{ s}^{-1}$. The loss rate A_1^m of the metastable ions relative to that of the ground state ions ($A_1^g \approx |X^-|$) was deduced from the ionization-rate measurement mentioned in sec.6.2. From the ratio of the ionization count rate right after the injection and after a few seconds, when practically all ions are in the ground state, and from the initial metastable fraction derived from the DR analysis of sec.5.4, we deduce $A_1^m/A_1^g = 2.1(8)$ and hence $A_1^m = 1.6(6) \cdot 10^{-2} \text{ s}^{-1}$.